AN INSIGHT INTO THE COMPARISON OF DIFFERENT MODELING METHODS FOR: SOIL STRUCTURE INTERACTION ANALYSIS OF DEEP FOUNDATIONS

Dr. Eng. Özgür BEZGİN

İSTANBUL
January 2010

TABLE OF CONTENTS

COMPARISON OF FEM WITH EXISTING ANALTICAL MODELS AND EXPERIMENTAL RESULTS

1.1 Introduction

In this chapter the FE model of the soil-structure system developed in chapter three will be compared with existing analytical models and experimental results.

The existing analytical models include: 1) The Winkler beam model (Spring model) where the soil is modeled as a series of independent springs at certain intervals along the depth of the shaft, 2) The LPILE model, which is a commercial program, engineered for deep-foundation analysis, and which makes use of the previously discussed subgrade reaction theory and p-y curves.

The work presented in this chapter is to compare the results obtained for the laterally loaded drilled shaft analyzed by the three dimensional finite element models with the soil modeled as a continuum, and by comparing them to the spring model, the LPILE and experimental data obtained from various field tests.

1.2 Analytical Comparison

In this section, the results from the 3D FE soil continuum models (Both the type-1 and type-2 models), for the lateral load analysis are compared with those from the spring FE model and the LPILE model. Details of the Winkler beam (spring model) can be found in book titled “An Insight into the Theoretical Background of SSI”.

The non-linear load-displacement characteristics of the soil were obtained using the API procedure. The depth of the effective soil layers in resisting lateral loads is related to the slenderness of the shaft. The API procedure provides results for this effective region only. For soil depths beyond 5D, the effectiveness of the soil layers in resisting lateral loads diminishes. It is seen in table 1.4 in book titled “An

Insight into the Theoretical Background of SSI" that the value of the coefficients A_1 and B_1 become constant beyond a depth to diameter ratio (x/B) of 5. Figure 1.1, 1.2 and 1.3 shows non-linear p-y curves obtained at various depths up to 6D of soil depth. Beyond these depths, the yield strength of the soil increases, and only the linear elastic part of the soil behavior is accounted for. Table 1.1 and 1.2 summarize the necessary parameters for the development of the p-y curves for the 100ft deep and 6ft diameter shaft, and the p-y values respectively.

The following parameters: ϕ=37°, γ=120pcf, K_o=0.4, n_h=50pci, B=6ft were used to generate the p-y curves. The tabulations for the 50ft deep shaft and the 20ft shaft are similar and therefore will not be shown. P-y curves for the other shaft depths such as 80ft, 60ft, 40t and 30ft have also been generated with the same procedure.

The load-displacement characteristics for the soil have been represented by the p-y curves for the FE spring model. The stress-strain relationship for the soil is specified for the 3D FE soil continuum model. For a given constant of subgrade reaction, the elastic modulus was assumed to vary linearly with depth for the cohesionless soil. The elastic perfectly plastic model for the soil requires the strain level where the plastic behavior will prevail. The ratio of p_k/y_k as well as the multiplication of n_h with depth is the elastic modulus value for that depth. The effective soil layer around the shaft for type-1 shaft was taken as 2.5D. In order to specify the strain level where the plastic behavior prevails, the value of y_k is divided by 2.5D.

Aside from verification purposes, there were two other reasons for the comparison of the models: 1) to examine the effect of soil shear coupling and 2) to examine the effect of soil selfweight deformation in the lateral load deformation of the shaft. To this end, both the type-1 FEM where the shear coupling can be observed, and type-2 FEM where the shear coupling and the soil selfweight deformations can be

observed are compared with the spring models and the LPILE model. The surface friction for the soil continuum model has not been included in the analysis in order to exclude its effect.

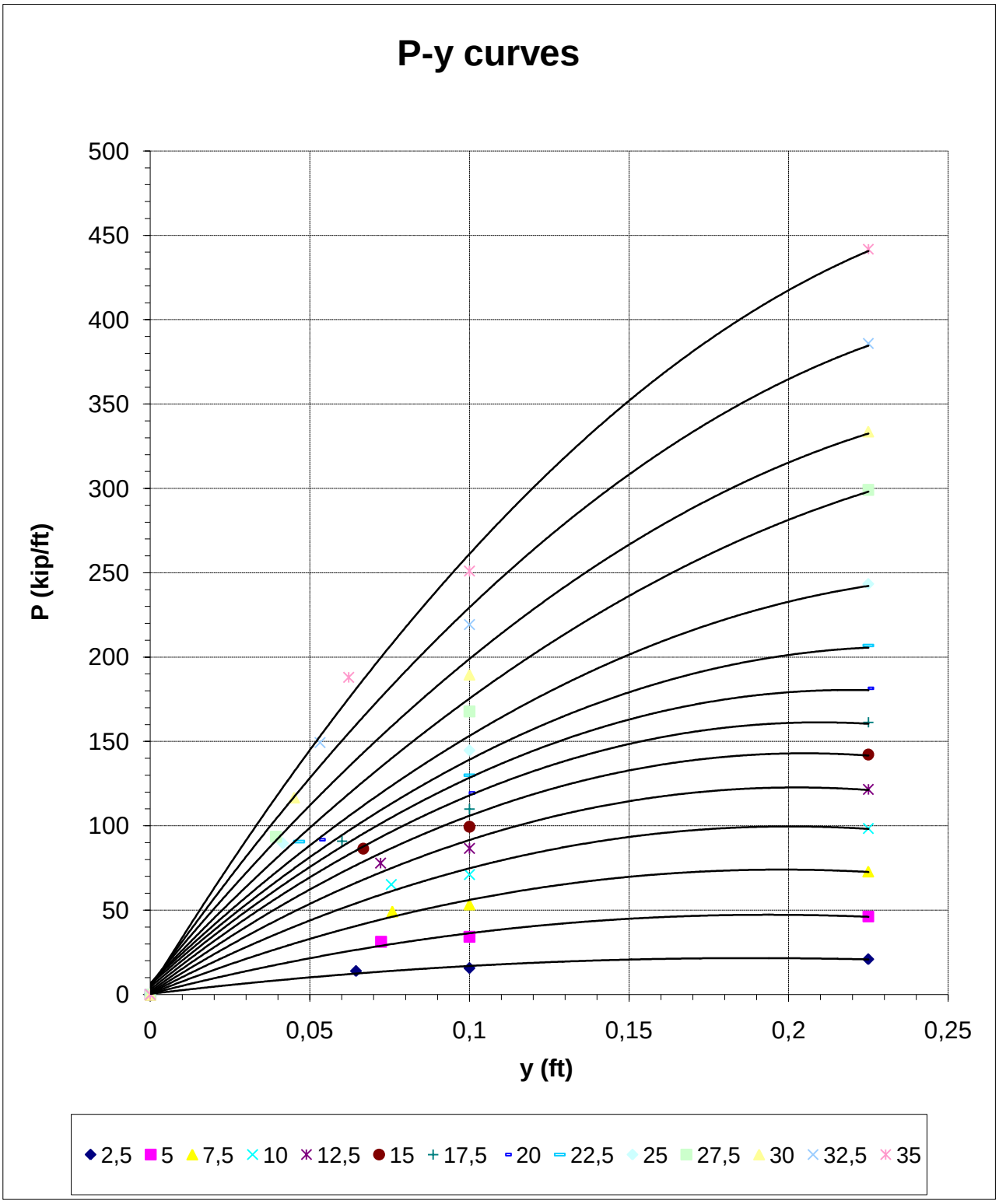

Figure 1.1 – p-y curves obtained by the API procedure for the effective zone of a 100ft deep 6ft diameter shaft in dense sand with n_h=50pci for various depths.

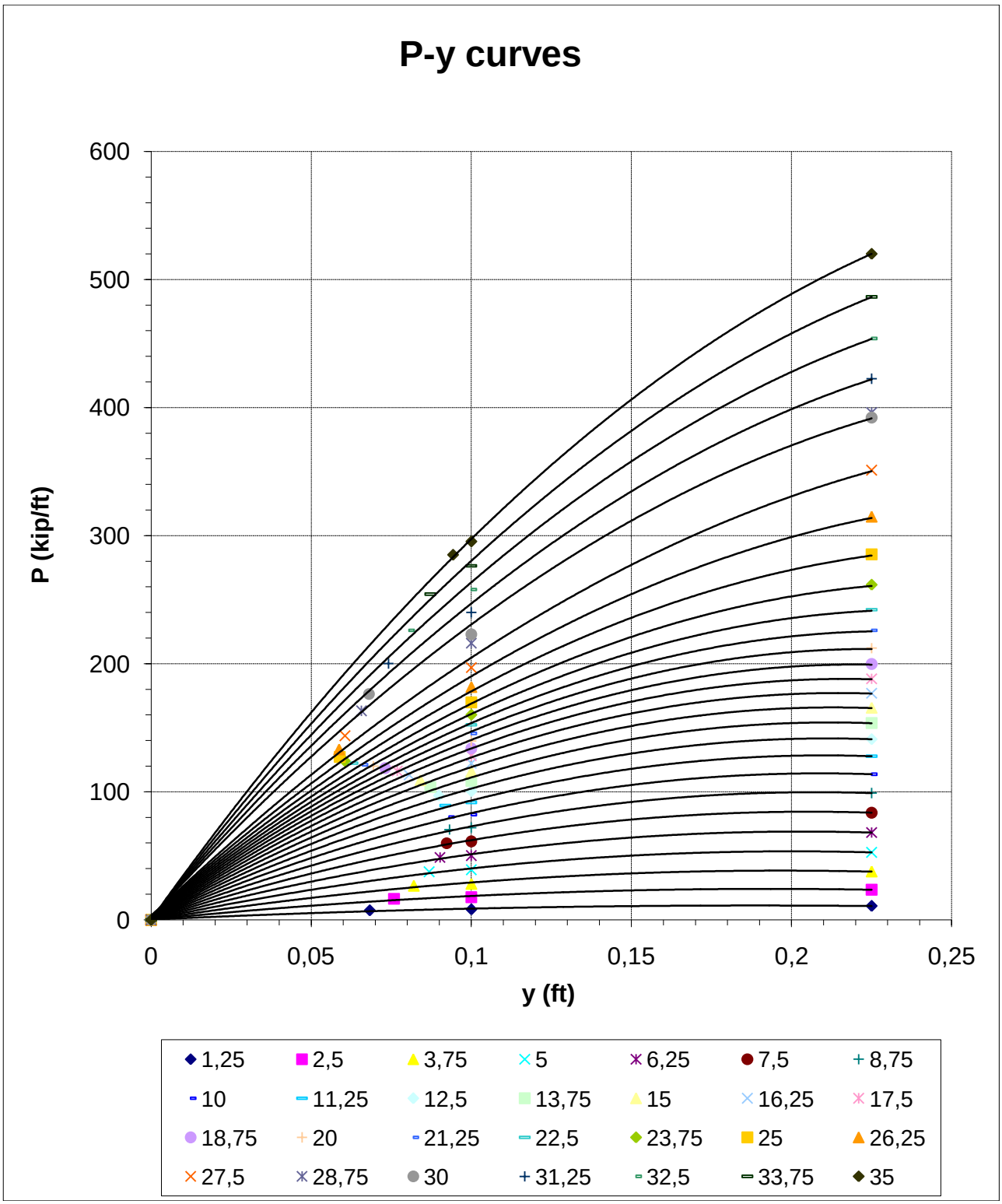

Figure 1.2 – p-y curves obtained by the API procedure for the effective zone of a 50ft deep 6ft diameter shaft in dense sand with n_h=50pci for various depths.

Table 1.1 - Parameters needed to generate API p-y curves for a 100ft deep shaft 6ft in diameter.

x (ft)	p_{cr}	p_{cd}	x/B	A	B	m	n	C
0	0.00	0.00	0	2.8688	2.175	0		
2.5	9.27	114.75	0.417	2.54151	1.903	47.323	3.728	32.72
5	23.61	229.50	0.833	2.232441	1.653	109.49	3.563	74.45
7.5	43.01	344.25	1.25	1.945542	1.424	179.59	3.41	120.30
10	67.49	459.00	1.667	1.684763	1.218	252.27	3.257	166.62
12.5	97.03	573.76	2.083	1.454053	1.035	324.92	3.092	211.56
15	131.64	688.51	2.5	1.257363	0.879	398.73	2.901	255.83
17.5	171.32	803.26	2.917	1.098641	0.749	479.83	2.673	303.52
20	216.07	918.01	3.333	0.981837	0.646	580.36	2.405	363.59
22.5	265.89	1032.76	3.75	0.910902	0.573	719.62	2.116	452.08
25	320.77	1147.51	4.167	0.889784	0.529	925.15	1.835	595.39
27.5	380.73	1262.26	4.583	0.922433	0.517	1233.9	1.596	833.35
30	445.75	1377.01	5	0.88	0.5	1355.1	1.645	903.77
32.5	515.84	1491.77	5.417	0.88	0.5	1568.1	1.645	1045.88
35	591.00	1606.52	5.833	0.88	0.5	1796.6	1.645	1198.27
37.5	671.22	1721.27	6.25	0.88	0.5	2040.5	1.645	1360.94
40	756.52	1836.02	6.667	0.88	0.5	2299.8	1.645	1533.88
42.5	846.88	1950.77	7.083	0.88	0.5	2574.5	1.645	1717.09
45	942.32	2065.52	7.5	0.88	0.5	2864.6	1.645	1910.58
47.5	1042.82	2180.27	7.917	0.88	0.5	3170.2	1.645	2114.35
50	1148.38	2295.02	8.333	0.88	0.5	3491.1	1.645	2328.40
52.5	1259.02	2409.78	8.75	0.88	0.5	3827.4	1.645	2552.72
55	1374.73	2524.53	9.167	0.88	0.5	4179.2	1.645	2787.32
57.5	1495.50	2639.28	9.583	0.88	0.5	4546.3	1.645	3032.19
60	1621.34	2754.03	10	0.88	0.5	4928.9	1.645	3287.34
62.5	1752.25	2868.78	10.42	0.88	0.5	5326.9	1.645	3552.77
65	1888.23	2983.53	10.83	0.88	0.5	5740.2	1.645	3828.47
67.5	2029.28	3098.28	11.25	0.88	0.5	6169	1.645	4114.45
70	2175.40	3213.03	11.67	0.88	0.5	6613.2	1.645	4410.71
72.5	2326.58	3327.79	12.08	0.88	0.5	7072.8	1.645	4717.24
75	2482.83	3442.54	12.5	0.88	0.5	7547.8	1.645	5034.05
77.5	2644.15	3557.29	12.92	0.88	0.5	8038.2	1.645	5361.14
80	2810.54	3672.04	13.33	0.88	0.5	8544.1	1.645	5698.50
82.5	2982.00	3786.79	13.75	0.88	0.5	9065.3	1.645	6046.14
85	3158.53	3901.54	14.17	0.88	0.5	9601.9	1.645	6404.05
87.5	3340.12	4016.29	14.58	0.88	0.5	10154	1.645	6772.24
90	3526.79	4131.04	15	0.88	0.5	10721	1.645	7150.71
92.5	3718.52	4245.80	15.42	0.88	0.5	11304	1.645	7539.45
95	3915.32	4360.55	15.83	0.88	0.5	11903	1.645	7938.47
97.5	4117.18	4475.30	16.25	0.88	0.5	12516	1.645	8347.77
100	4324.12	4590.05	16.67	0.88	0.5	13145	1.645	8767.34

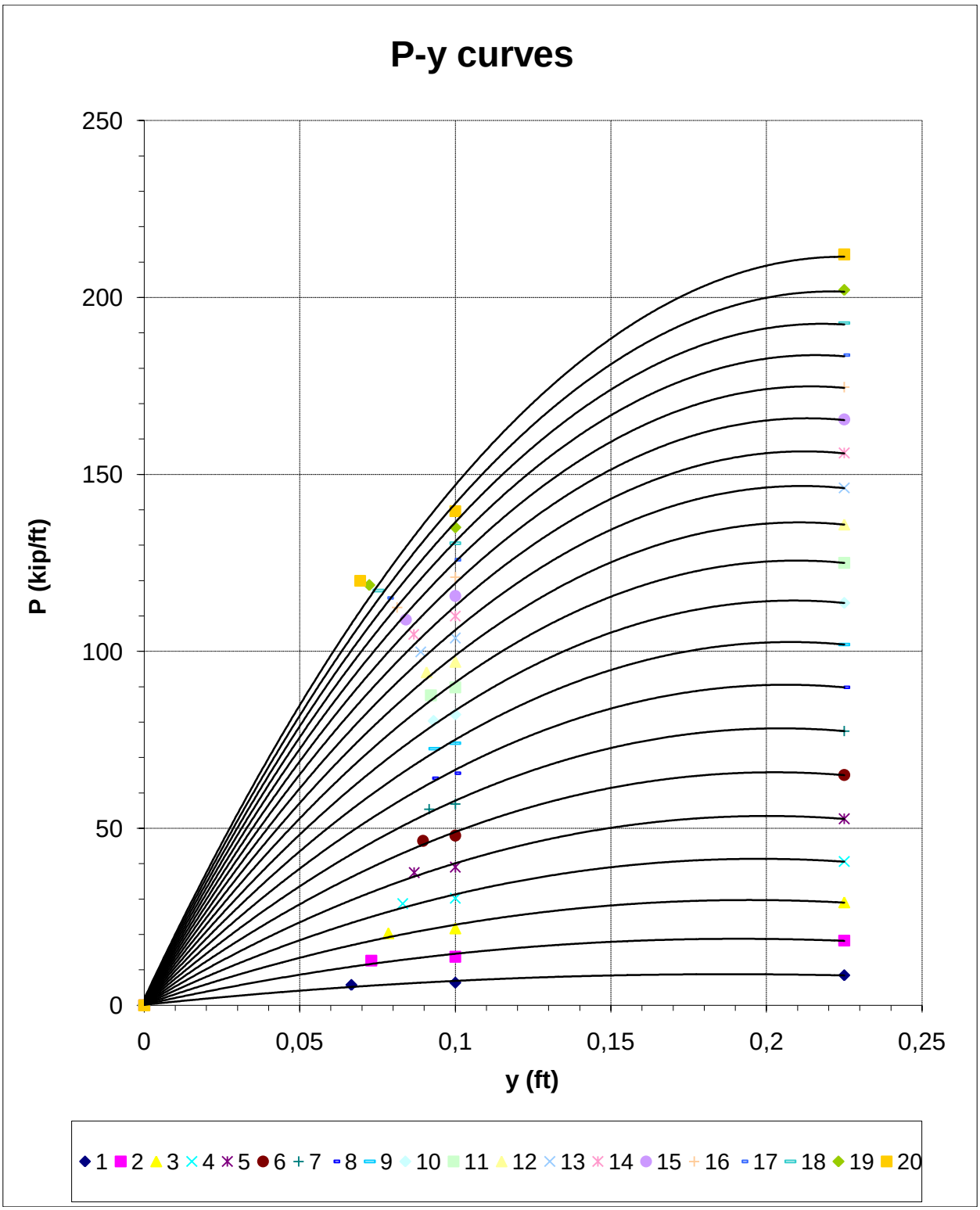

Figure 1.3 –p-y curves obtained by the API procedure for 20ft deep 6ft diameter shaft in dense sand with n_h=50pci for various depths.

Table 1.2 – Non-linear p-y curves and material properties for the soil layers.

				P-Y CURVE VALUES					
	Elastic modulus (ksf)	Yield stress (ksf)	Yield strain	Reaction per ft (kip/ft)			Displacement (ft)		
Depth (ft)				p_u	p_m	p_k	y_u	y_m	y_k
0	0	0.0	0.0000	0.00	0.00	0.00	0.225	0.1	0.00
2.5	216	1.1	0.0051	23.56	17.64	16.38	0.225	0.1	0.076
5	432	2.5	0.0058	52.70	39.02	37.50	0.225	0.1	0.087
7.5	648	4.0	0.0062	83.69	61.24	59.82	0.225	0.1	0.092
10	864	5.4	0.0062	113.70	82.17	80.36	0.225	0.1	0.093
12.5	1080	6.5	0.0060	141.09	100.47	97.06	0.225	0.1	0.090
15	1296	7.3	0.0056	165.52	115.68	108.97	0.225	0.1	0.084
17.5	1512	7.7	0.0051	188.22	128.24	116.22	0.225	0.1	0.077
20	1728	8.0	0.0046	212.15	139.60	119.94	0.225	0.1	0.069
22.5	1944	8.2	0.0042	242.20	152.25	122.29	0.225	0.1	0.063
25	2160	8.5	0.0039	285.42	169.78	127.25	0.225	0.1	0.059
27.5	2376	9.6	0.0040	351.19	196.96	143.80	0.225	0.1	0.061
30	2592	11.8	0.0045	392.26	222.87	176.34	0.225	0.1	0.068
32.5	2808	15.1	0.0054	453.94	257.92	226.06	0.225	0.1	0.081
35	3024	19.0	0.0063	520.08	295.50	285.10	0.225	0.1	0.094
37.5	3240	23.6	0.0073			354.45			0.11
40	3456	29.0	0.0084			435.13			0.13
42.5	3672	35.2	0.0096			528.19			0.14
45	3888	42.3	0.0109			634.72			0.16
47.5	4104	50.4	0.0123			755.85			0.18
50	4320	59.5	0.0138			892.73			0.21
52.5	4536	69.8	0.0154			1046.55			0.23
55	4752	81.2	0.0171			1218.51			0.26
57.5	4968	94.0	0.0189			1409.87			0.28
60	5184	108.1	0.0209			1621.89			0.31
62.5	5400	123.7	0.0229			1855.88			0.34
65	5616	140.9	0.0251			2113.17			0.38
67.5	5832	159.7	0.0274			2395.10			0.41
70	6048	180.2	0.0298			2703.08			0.45
72.5	6264	202.6	0.0323			3038.50			0.49
75	6480	226.9	0.0350			3402.80			0.53
77.5	6696	253.2	0.0378			3797.45			0.57
80	6912	281.6	0.0407			4223.94			0.61
82.5	7128	312.3	0.0438			4683.77			0.66
85	7344	345.2	0.0470			5178.49			0.71
87.5	7560	380.6	0.0503			5709.66			0.76
90	7776	418.6	0.0538			6278.86			0.81
92.5	7992	459.2	0.0575			6887.70			0.86
95	8208	502.5	0.0612			7537.83			0.92
97.5	8424	548.7	0.0651			8230.89			0.98
100	8640	597.9	0.0692			8968.57			1.04

Comparisons of results from the various models were made for the following shaft depths (H): 100ft, 80ft, 60ft, 50ft, 40ft, 30ft and 20ft with a 20ft column height and 6 ft diameter. In order to isolate the effect of fixed support conditions, the shafts were supported on very stiff soil at the bottom with no friction. Four models were compared: 1) Spring model, 2) LPILE, 3) Type-1 FEM, 4) Type-2 FEM. The notation FEM* will be used to define the type-2 finite element continuum model and the notation FEM will be used to define the type-1 finite element model continuum model. Figures 1.4, 1.5 and 1.6 show the variation of displacements, moments and shears for 100ft, 80ft, 60ft, 50ft, 40ft, and 30ft shafts. In all these figures, the spring model and the LPILE overestimated the shaft displacements, moments and shears. Differences have been observed in the value as well as the location of maximum moment. The shear value was at the highest value at the ground level except for the 30ft and 20ft deep shafts. In these figures, the results estimated by the LPILE was the highest and the results estimated by the FEM* were the lowest. The displacements, moments and shears from the FEM* and the spring model for the various shaft depths are shown in figures 1.7, 1.8 and 1.9 respectively. These figures show the combined effect of shear coupling and selfweight deformations on the shaft response.

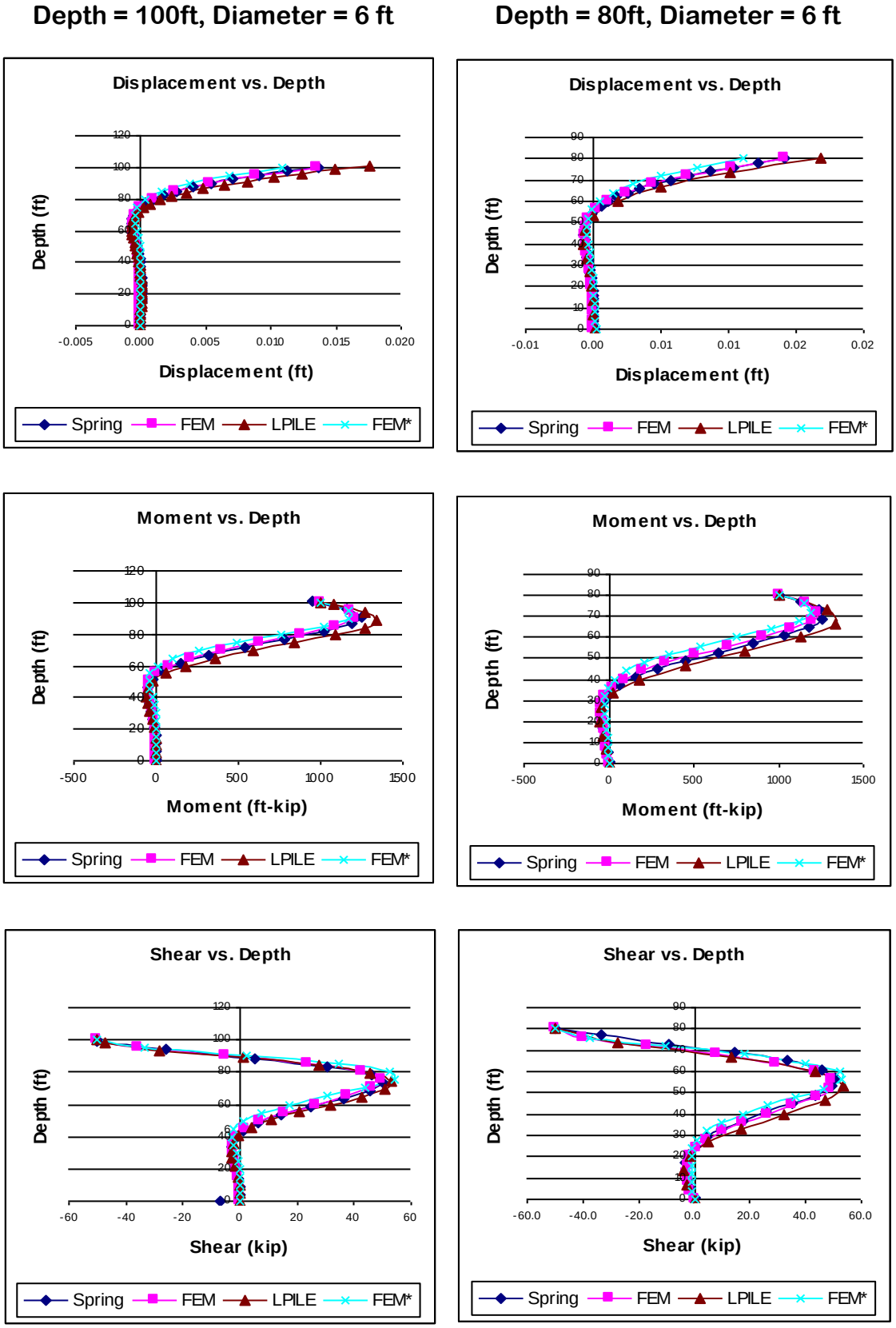

Figure 1.4 – Displacement, moment and shear diagrams for 100ft and 80ft deep shafts

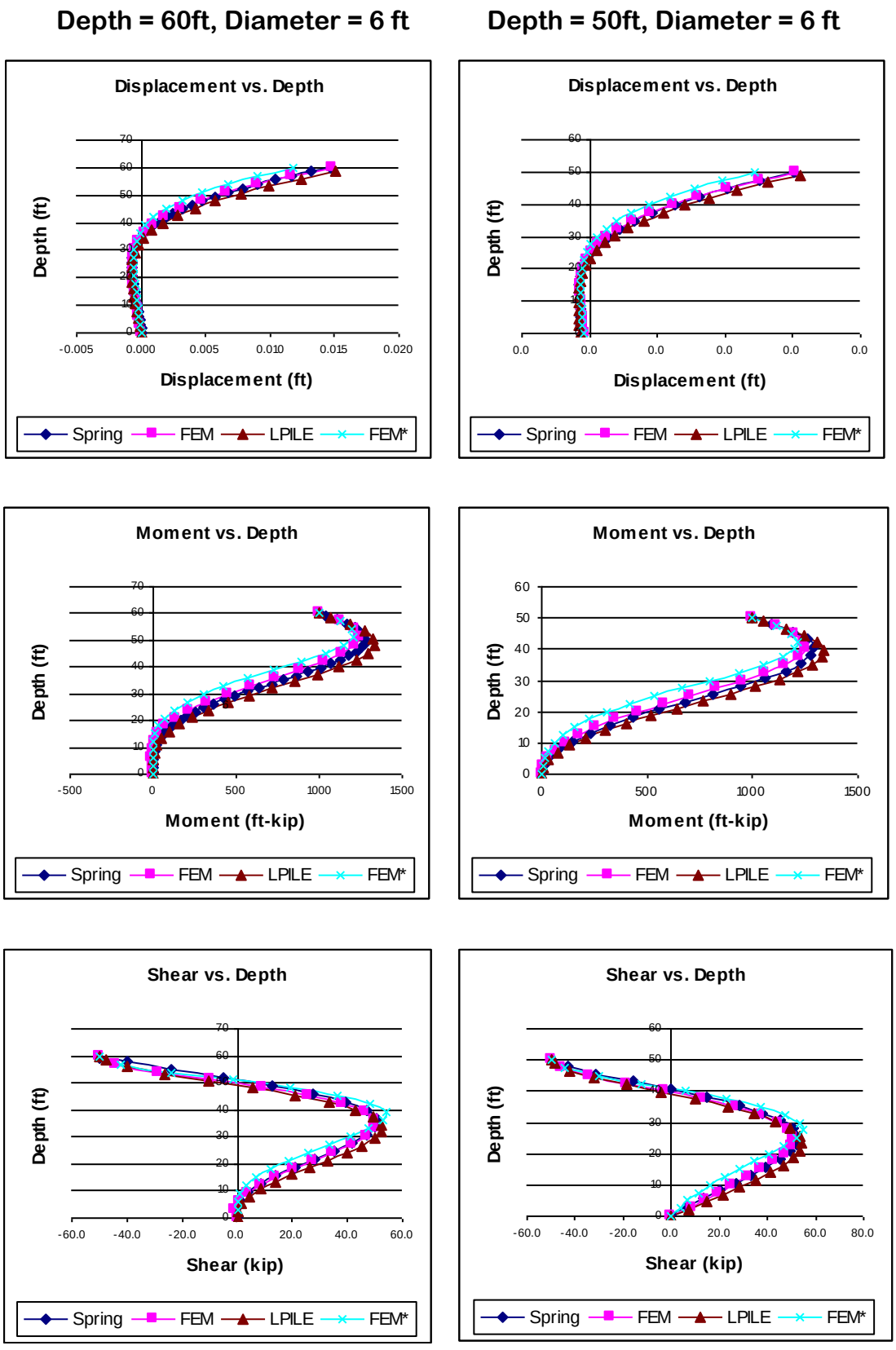

Figure 1.5 – Displacement, moment and shear diagrams for 60ft and 50ft deep shafts.

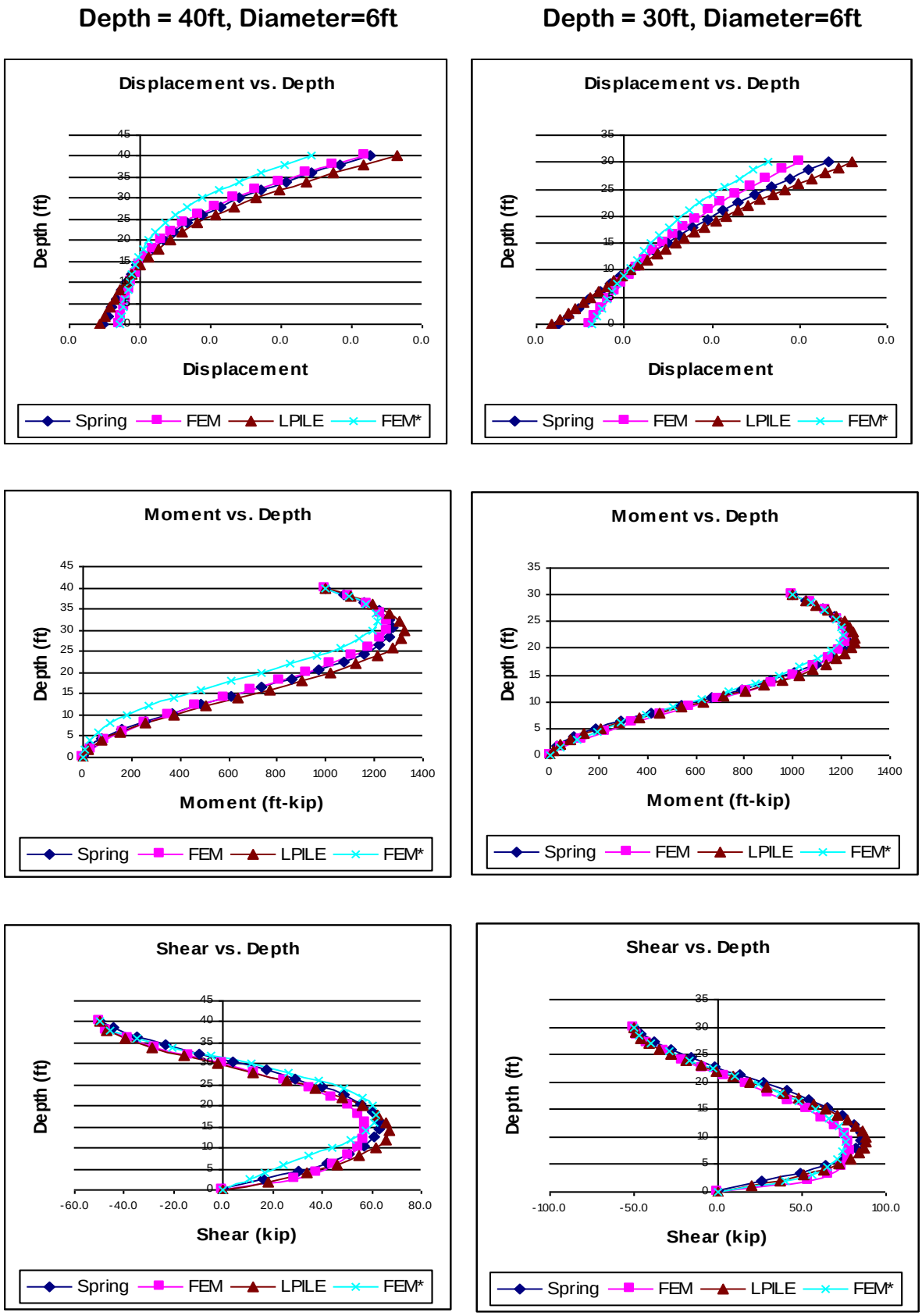

Figure 1.6 –Displacement, moment and shear diagrams for 40ft and 30ft deep shafts.

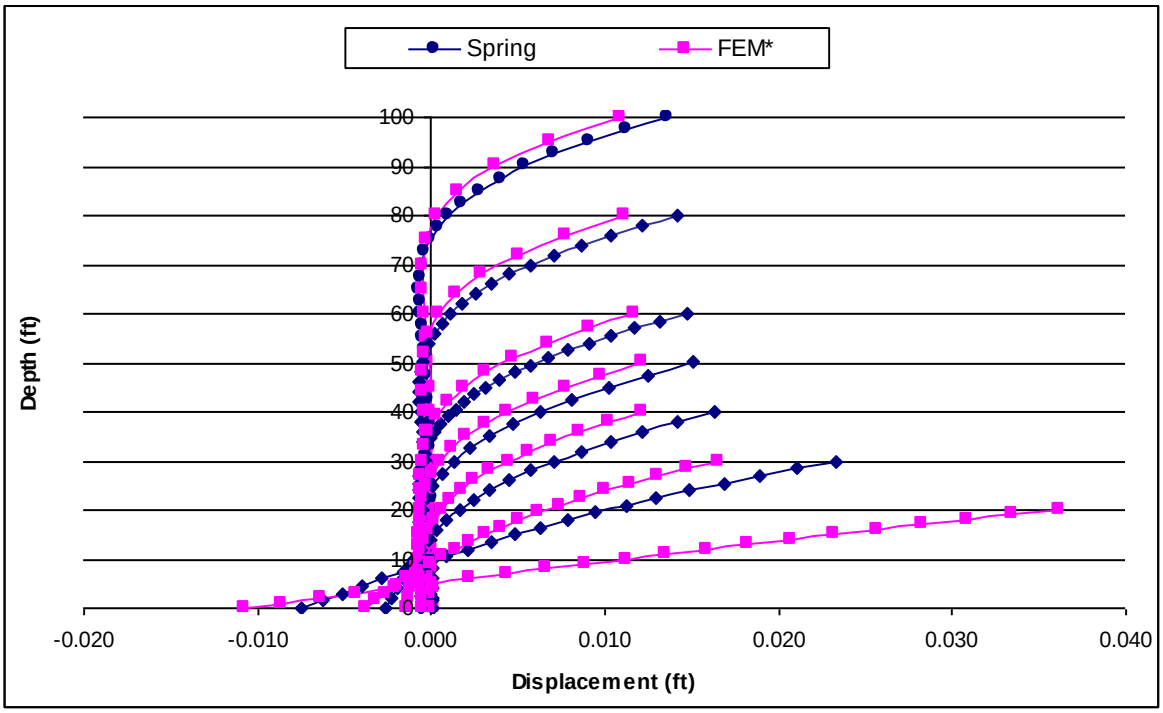

Figure 1.7 – Variation of displacement for the spring model and the 3D soil continuum model, for various shaft depths.

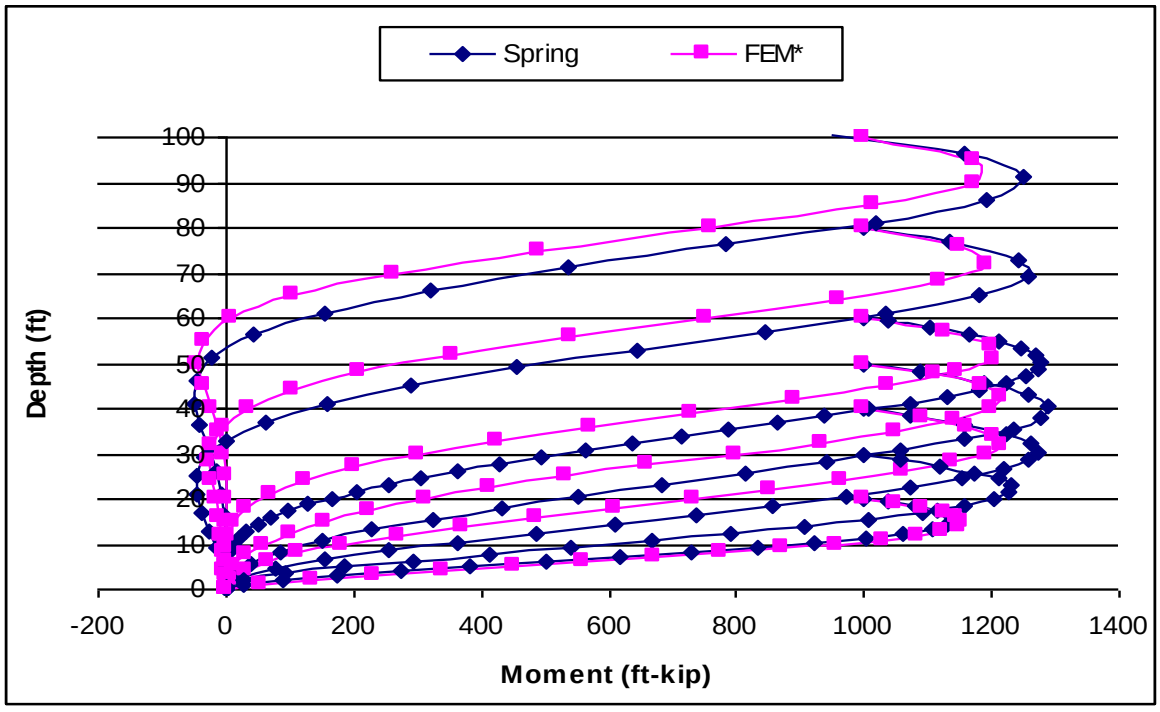

Figure 1.8 –Variation of moment for the spring model and the 3D soil continuum model, for various shaft depths.

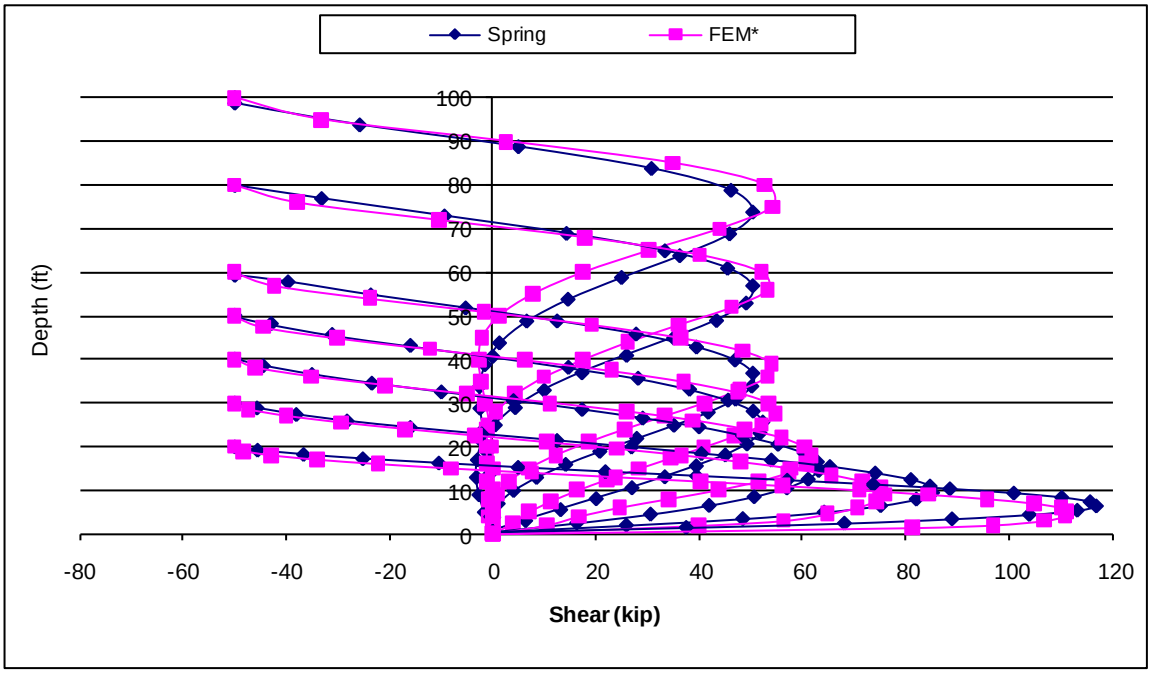

Figure 1.9 – Variation of shear for the spring model and soil continuum model, for various shaft depths.

Figure 1.10 shows the maximum displacements as a function of the shaft depth to diameter ratio from various models. In order to see the effect of the model type on the displacement, the displacement values were normalized with respect to type-2 FEM displacement results, which are presented in figure 1.11. The subgrade reaction theory predicts displacement results that are approximately 25% higher than the FEM*. As the shaft depth becomes smaller, the selfweight deformation effects on the lateral response also become smaller, thus the difference between the FEM* and FEM plots becomes smaller. The LPILE and the spring models represent the normal support of the stiff soil layer to the 6 ft diameter shaft by a roller, as the depth of the shaft is decreased the amount of lateral movement predicted by the spring and the LPILE becomes significantly larger. In the extreme case, as the depth decreases to 0, since the soil support is completely diminished and since the shafts are roller supported, displacements will go to infinity.

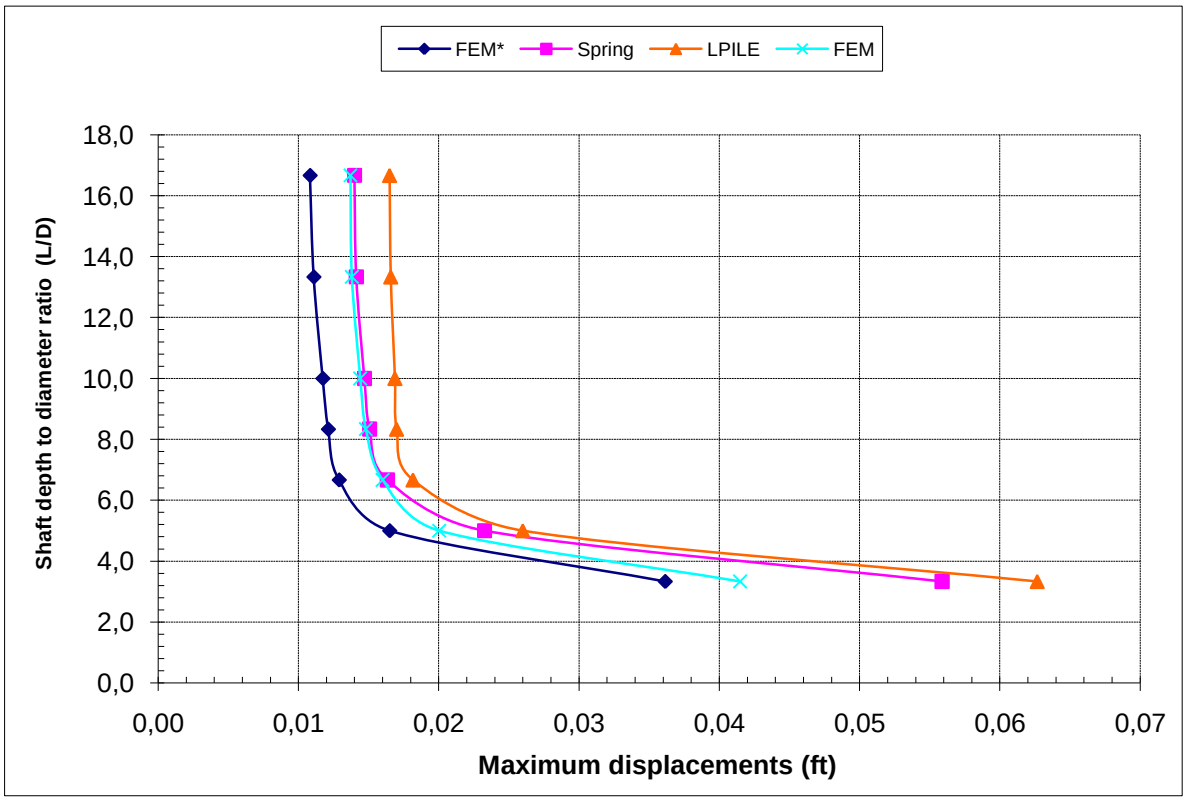

Figure 1.10 – Variation of maximum displacements with shaft depth to diameter ratio from various models.

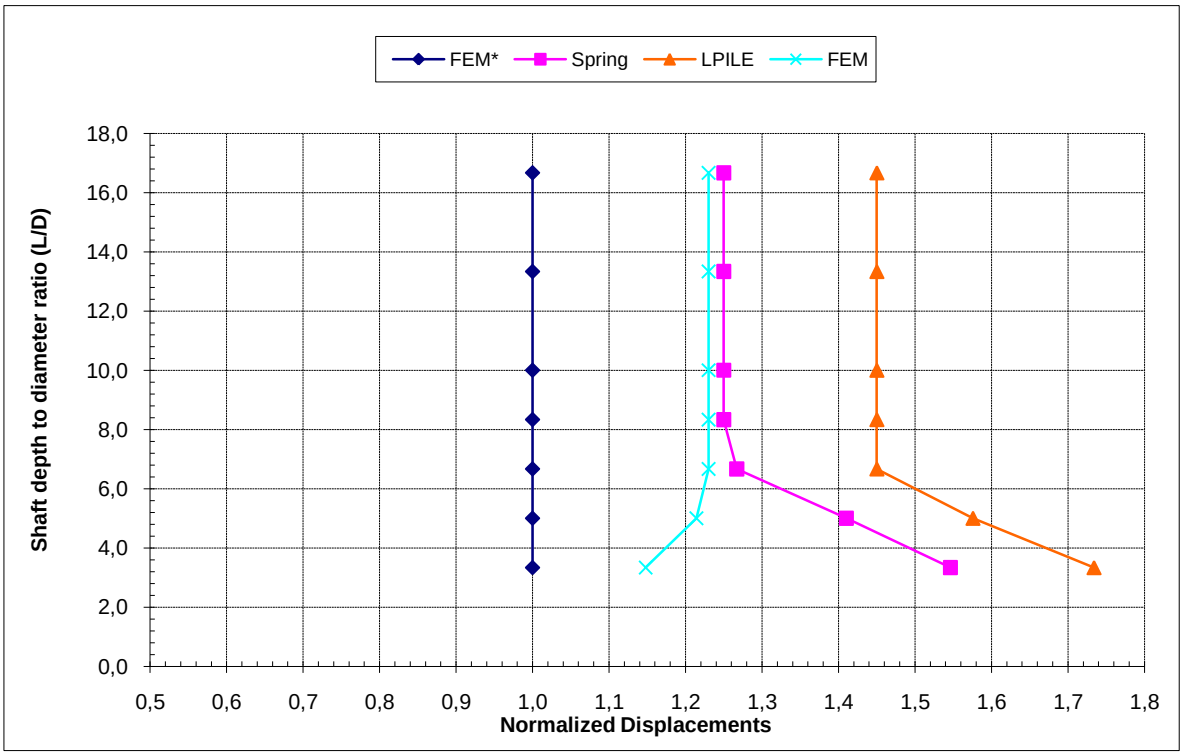

Figure 1.11 –Variation of normalized displacements with shaft depth to diameter ratio from various models.(Normalized with respect to FEM*).

Figure 1.10 and 1.11 show that maximum displacement predicted by the Winkler beam model (spring model) and LPILE are higher than those from the 3D FE soil continuum developed in this study. This suggests that the spring model has less stiffness than the 3D FE models.

Normalizing the maximum displacement values with respect to the displacement of the deepest shaft i.e. that of 100ft deep 6 ft diameter shaft shows the effect of shaft depth and relative stiffness on lateral load capacity. Figure 1.12 shows the percentage increase in displacements as the shaft depth is decreased. Figure 1.12 also shows that the change in maximum displacement value is not significant for depth to diameter ratios higher than 12.5. The effective shaft depth in lateral load capacity of a deep shaft was discussed in section 1.6.1.1 of book titled "An Insight into the Theoretical Background of SSI where equation (36) referred to the relative stiffness of the shaft and soil, and the maximum depth coefficient Z_{max}, referred to the effectiveness of the shaft depth for resisting lateral loads. For $Z_{max} \geq 5$, the shafts were considered long (Matlock and Reese 1961, 1962) and further increase in shaft depth did not change the lateral load capacity. The relative stiffness factor was determined as $T=(EI/n_h)^{1/5}$, and maximum depth coefficient as $Z_{max}=L/T$.

The relative stiffness of the SSI system, the depth coefficients and the slenderness values of the shafts are tabulated in table 1.3. Shaft depths below 65ft have Z values below 5, which places them in the transition zone between the slender behavior and rigid behavior ($2 < Z < 5$) according to Matlock and Reese.

Table 1.3 – Relative stiffness and depth coefficients of the shafts.

Diameter(ft)=	6
I (ft^4) =	63.62
E (ksf) =	518400
n_h (kcf)=	86.4
T =	156.87

Depth (ft)	Z_{max}	L/D
100.0	7.7	16.7
80.0	6.1	13.3
60.0	4.6	10.0
50.0	3.8	8.3
40.0	3.1	6.7
30.0	2.3	5.0
20.0	1.5	3.3

Table 1.4 shows the percentage increase in maximum displacements predicted by the various models as the shaft slenderness decreases. Note that there is a significant increase in maximum displacements below the depth of 60ft.

These results are in agreement with the Matlock and Reese equation, which states that, the shafts with depth coefficients (L/T) 5 or more have the same resistance to lateral load.

Table 1.4 – Percentage increase in maximum displacement from various models.

		Normalized displacements with respect to L/D1=16.7 for various models.			
L (ft)	L/D	Spring	FEM	FEM*	LPILE
100	16.7	1.00	1.00	1.00	1.00
80	13.3	1.01	1.01	1.02	1.01
60	10.0	1.05	1.05	1.08	1.02
50	8.3	1.08	1.08	1.12	1.03
40	6.7	1.17	1.17	1.19	1.10
30	5.0	1.66	1.46	1.52	1.58
20	3.3	3.99	3.03	3.34	3.80

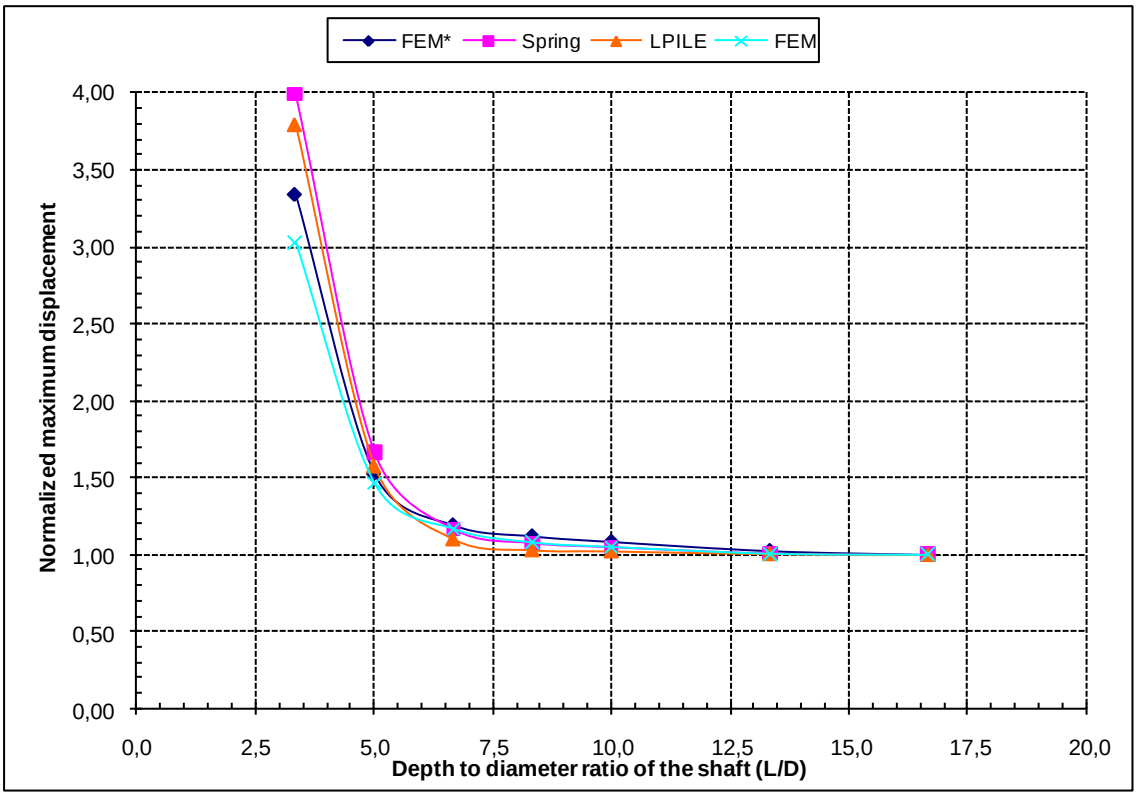

Figure 1.12 – Variation of normalized maximum displacement with shaft depth to diameter ratio from various models (Normalized with respect to maximum L/D).

Figure 1.13 shows the variation of maximum moments with shaft depth to diameter ratio predicted by various models. The moment is increased down to a certain depth by the increasing displacements where the bending deformation prevails. However, a sudden shift at a depth to diameter ratio of 8 and depth coefficient value of 3.7 takes place. This is the point where the bending deformations change into rigid body motion. Due to decrease in curvature of the shaft, the moments decrease as well. Since the shafts are not fixed supported, the rigid body motion is not prevented. In other words, the depth to diameter ratio of 8 can also be viewed as the point where the support conditions become a factor in the lateral response characteristics of the shaft.

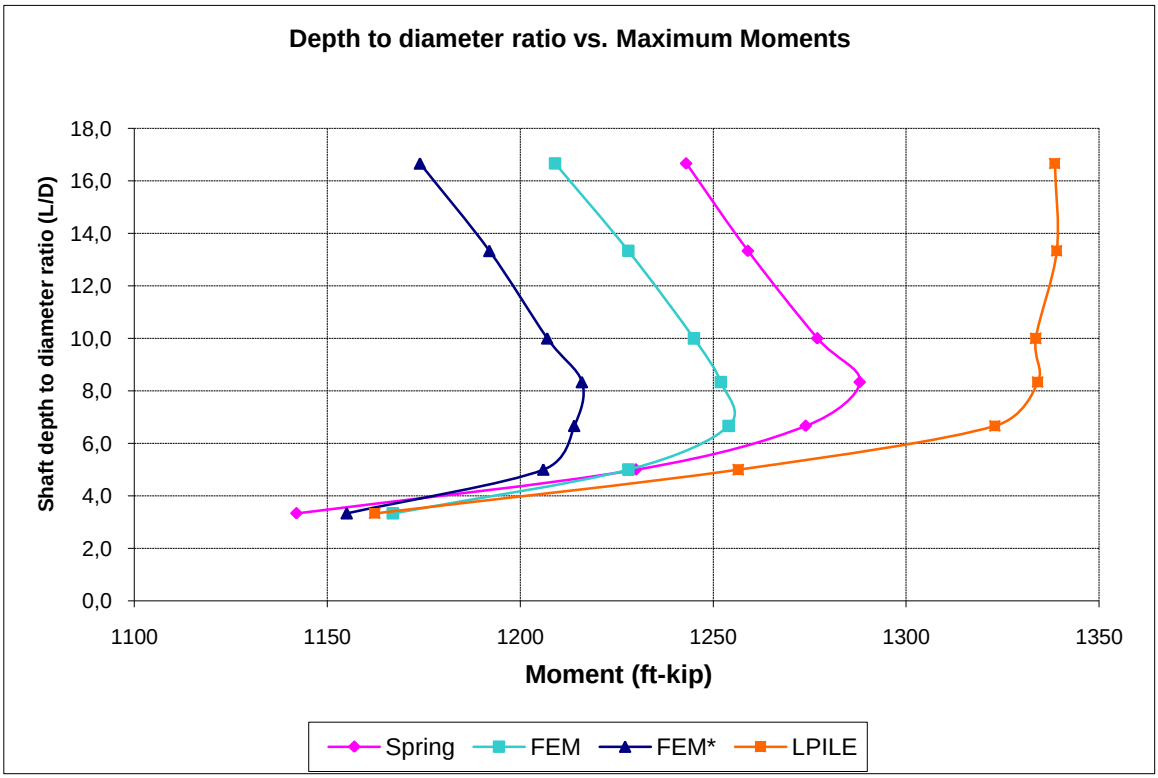

Figure 1.13 – Variation of maximum moments with shaft depth to diameter ratio.

Figure 1.14 is the normalized version of figure 1.13 where the moments for various depth to diameter ratios are normalized with respect to the FEM*. This figure shows the variation of maximum moments from various models compared to the 3D FE continuum model including soil weight.

From figure 1.14, as the FEM and the spring model results are compared, the shear coupling results in a 3% decrease in moment. Including the selfweight of the soil in the analysis (FEM*), results in another 3% decrease, resulting in 6% difference in maximum moment compared to the spring model.

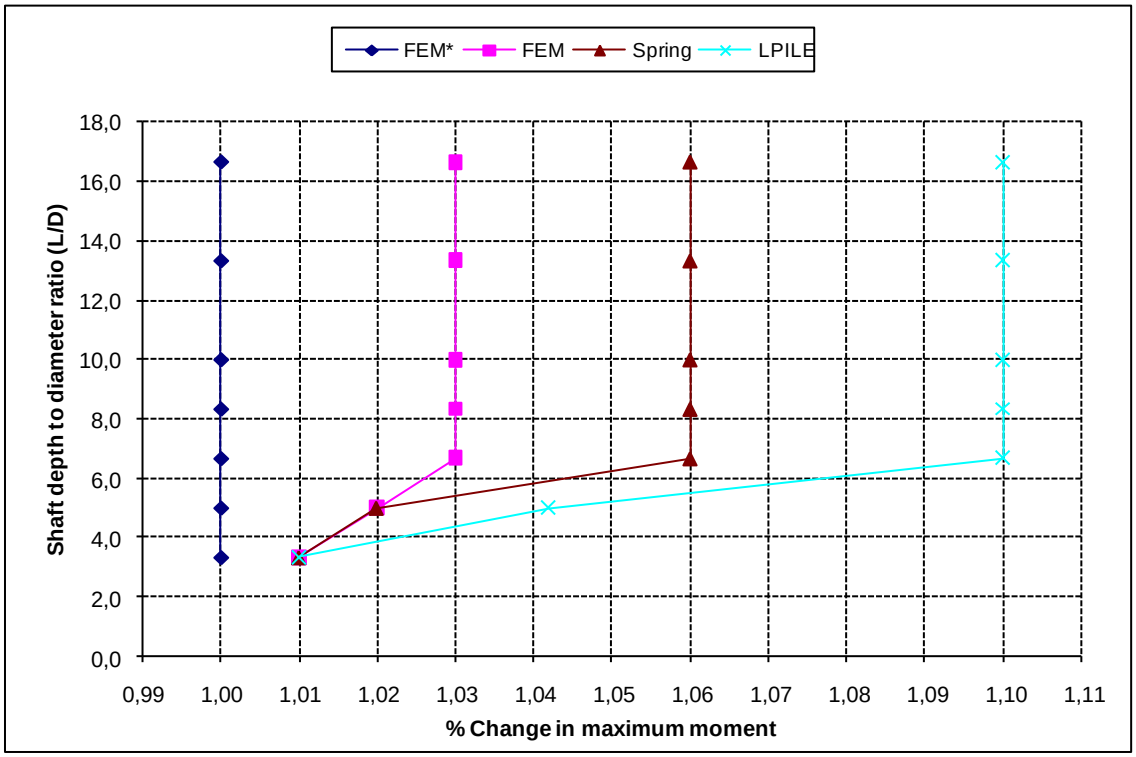

Figure 1.14 – Variation of normalized maximum moments with shaft depth to diameter ratio for various models (Normalized with respect to FEM*).

In order to verify the effect of support conditions, analysis have been conducted for 80ft, 50ft, 30ft and 20ft shaft with fixed supports. Figure 1.15 and 1.16 shows the variation of displacement, moment and shear for the 80ft and 50ft shafts.

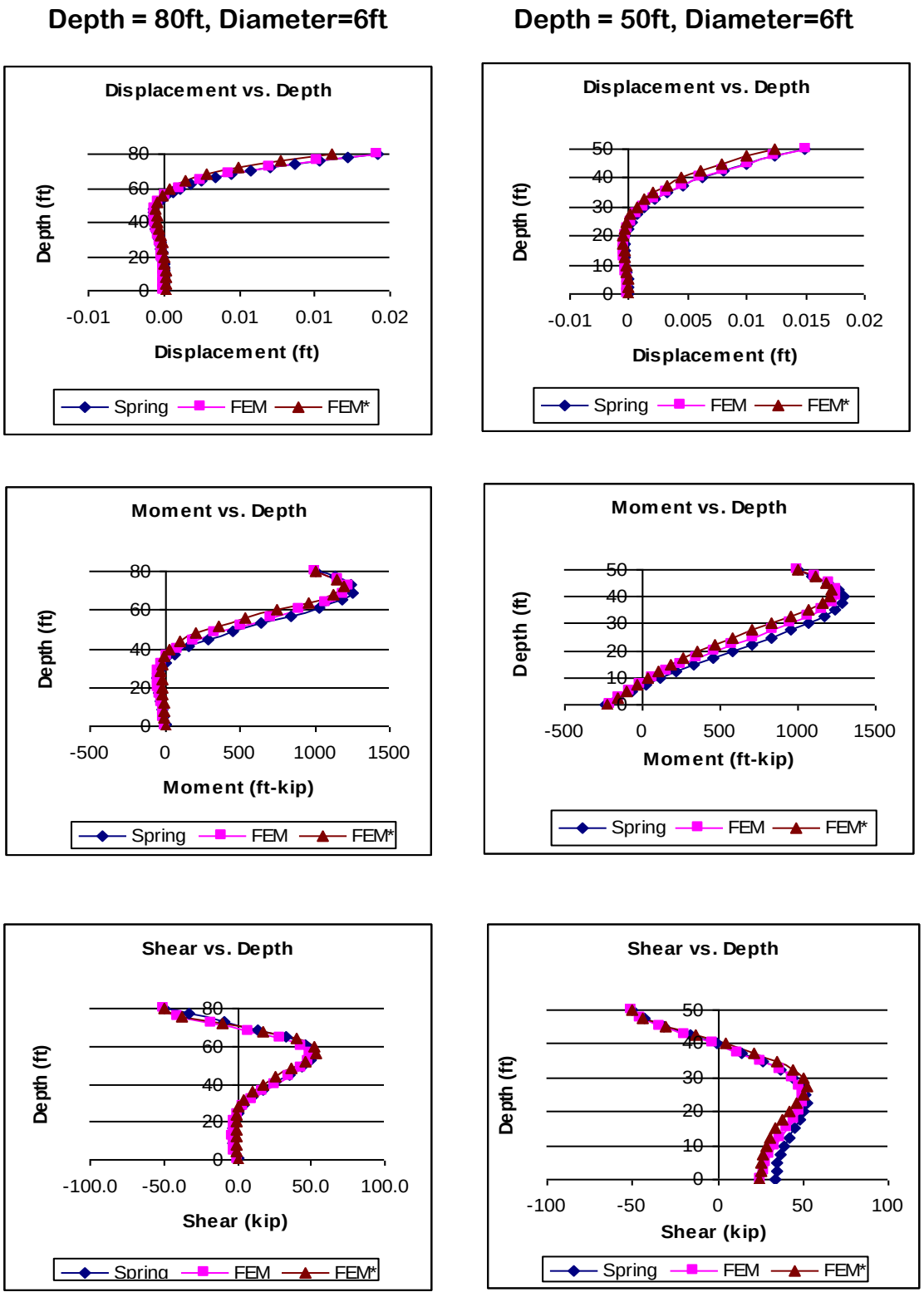

Figure 1.15 – Displacement, moment and shear diagrams for 80ft and 50ft deep shafts.

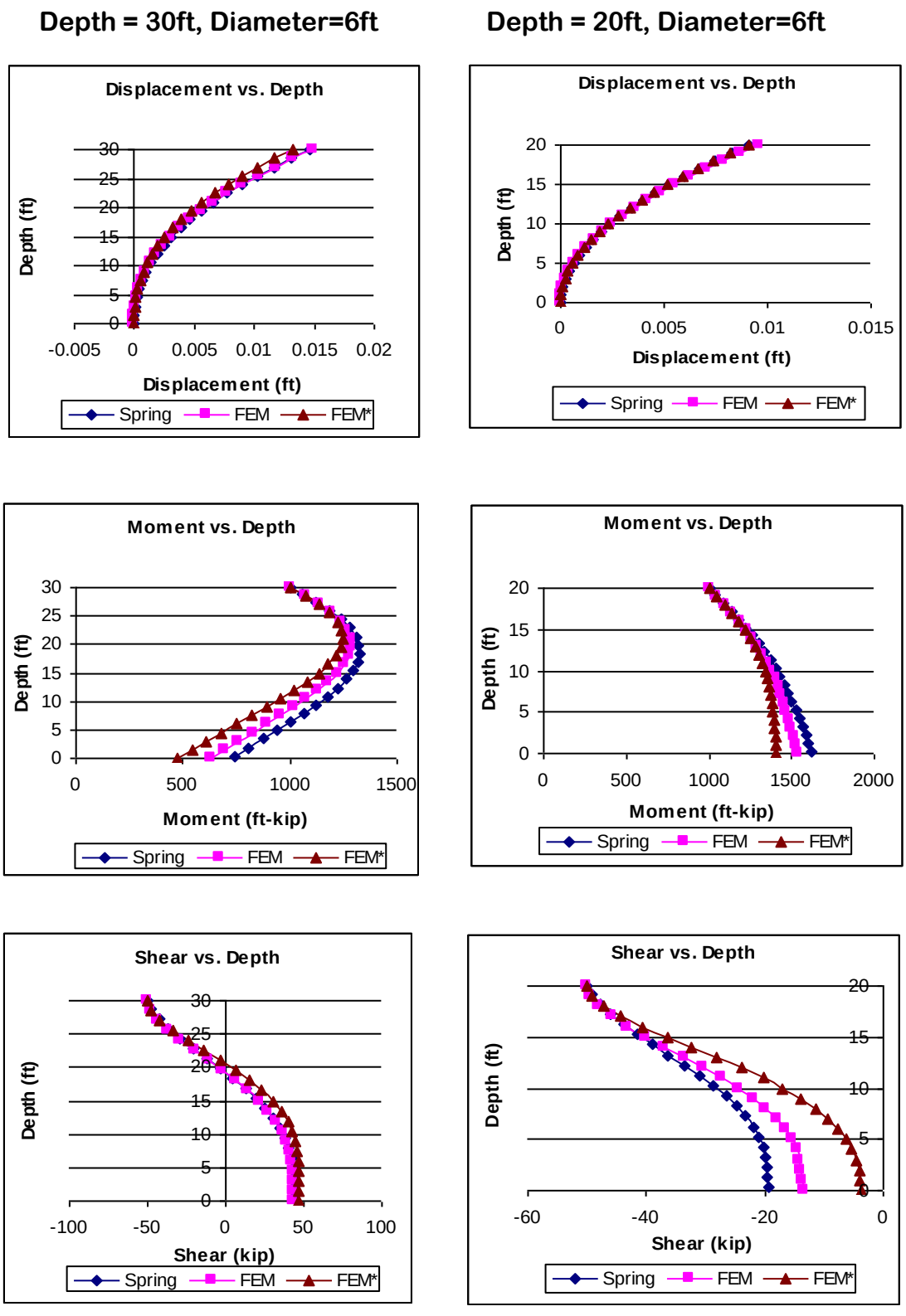

Figure 1.16 – Displacement, moment and shear diagrams for 30ft and 20ft deep shafts.

Figures 1.17 and 1.18 show the variation of maximum displacements with shaft depth to diameter ratio normalized with respect to the FEM*.

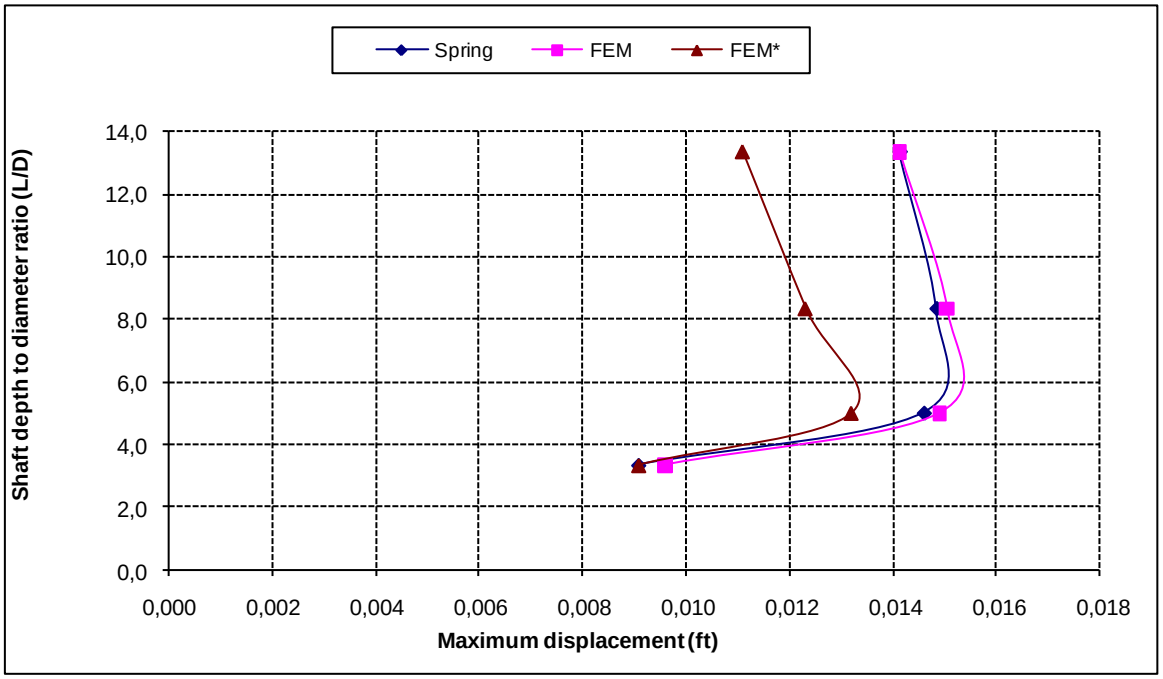

Figure 1.17 – Variation of maximum displacements with shaft depth to diameter ratio.

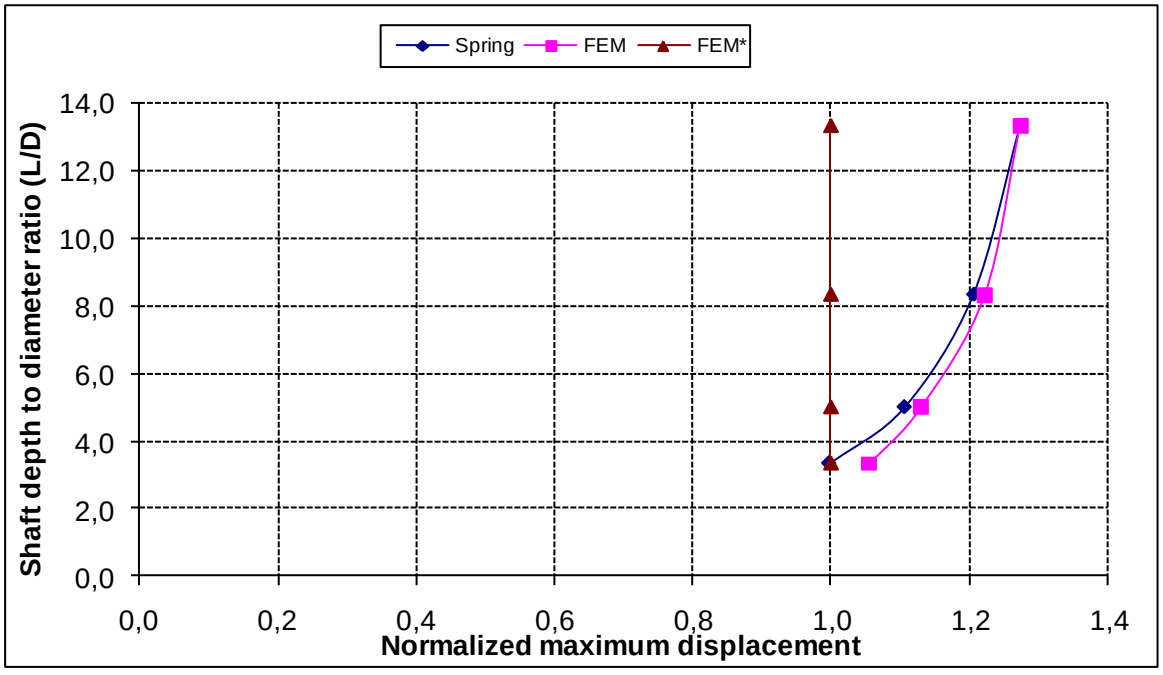

Figure 1.18 – Variation of maximum normalized displacements with shaft depth to diameter ratio (Normalized with respect to FEM*) for various models.

Figure 1.19 and 1.20 shows the variation of maximum moment with slenderness and normalized values with respect to type-2 fem.

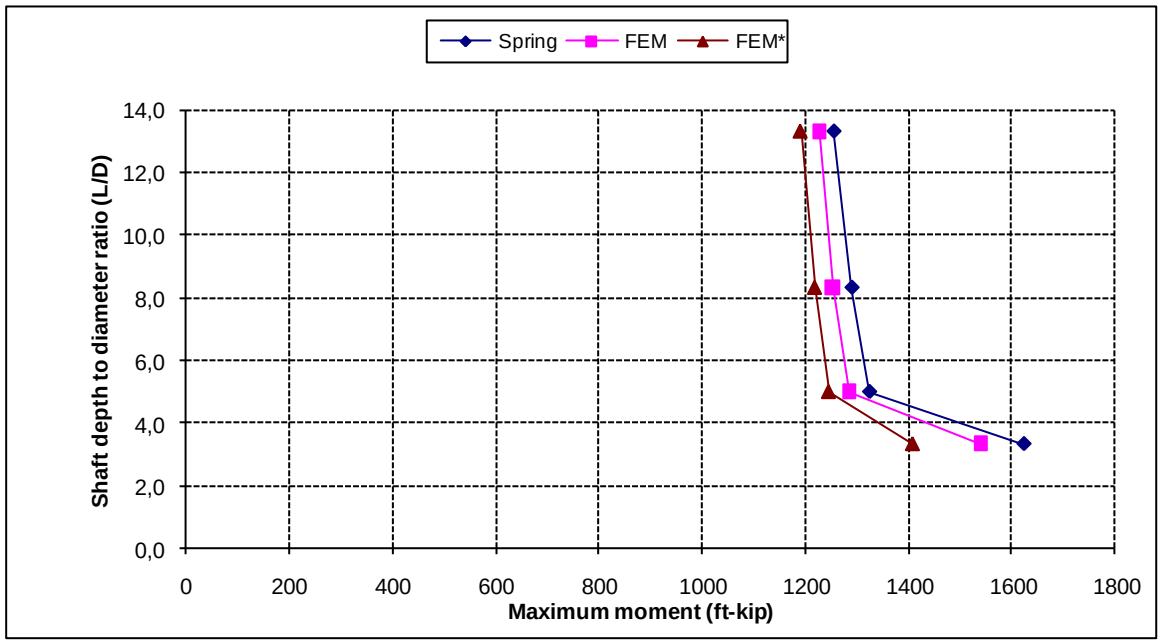

Figure 1.19 – Variation of maximum moments with shaft depth to diameter ratio for various models.

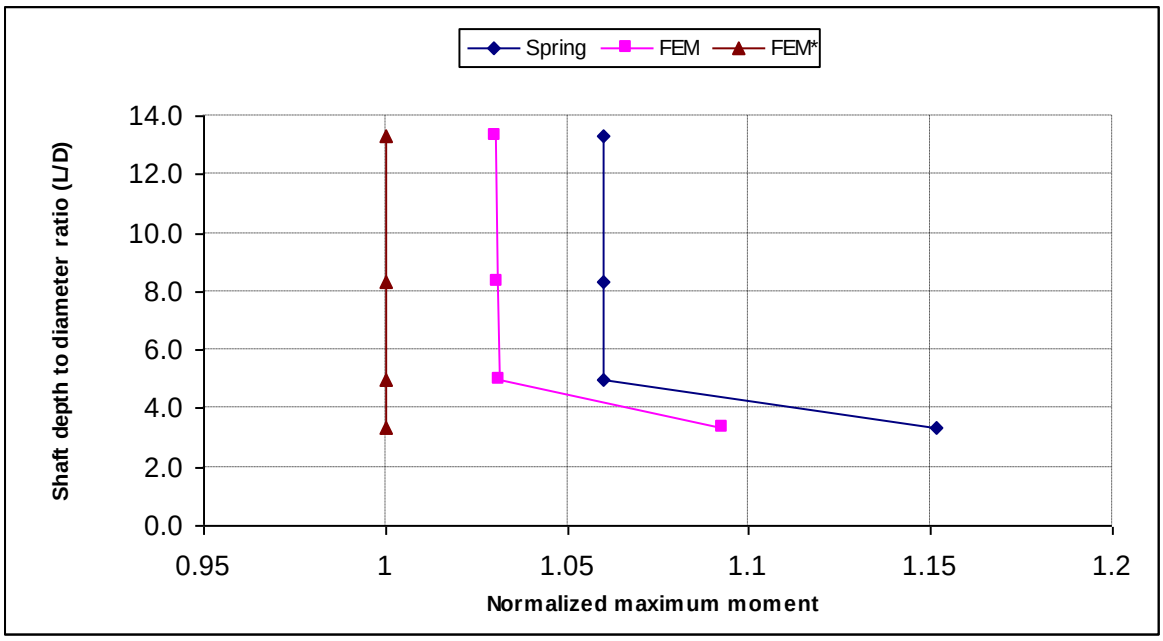

Figure 1.20 – Variation of normalized moments with shaft depth to diameter ratio (Normalized with respect to FEM*) for various models.

The change of support condition from normal support to fixed support has changed the variation of the maximum displacement and moment values with depth. As the shaft depth is decreases the lateral soil support decreases as well

and the support conditions start to influence the shaft behavior. Because of the fixed support, rigid body-like motion is not possible. Thus as the depth is decreased, the displacements approach to zero. Support to lateral loading, is a combination of shaft support and the soil support. For low shaft depths, the soil support is minimized and the fixed supported shaft is the primary element resisting the lateral loads. In figure 1.13 the shaft moments diminish due to rigid body-like motion and approach to zero. However, in figure 1.19 an opposite behavior is observed, since the shaft resists a greater share of the lateral load as the soil depth decreases.

Comparisons between the 3-D FE soil models and the spring models have shown that the spring model predicts higher displacements and moments. The study showed that the inclusion of the soil selfweight deformations within the analysis increases the capacity of the shaft. The comparison of the spring model and the FEM* showed that the location of the maximum moment predicted by the FEM* is closer to the ground surface, than the location predicted by the spring model. This is important for seismic design where the location and magnitude of the maximum moment is important for displacement-based design in seismic zones. The distance between the plastic hinge and the ground surface affects the displacement capacity of the structure and its effective vibration period. From figure 1.8 it is seen that the location of the maximum moment varies by approximately 8% along the depth of the shaft.

1.3 Experimental Verification

1.3.1 Lateral Load Tests on Small Diameter Drilled Piers (Kumar et.al 2004)

Kumar et.al (2004) tested small diameter drilled shafts under lateral loads using different concrete mix designs. They published a paper titled “Lateral Load Tests

on Small Diameter Drilled Piers" (Kumar, Kort, Hosin, and Chong 2004). Their tests compared the response of 25 ft deep and 13 inch in diameter shafts made of conventional concrete and coal combustion products (CCP). Use of coal in generation of electricity has resulted in production and accumulation of large quantities of coal combustion products (CCPs). The experiment involved the lateral load testing of a total of four shafts. Two shafts were constructed using conventional concrete and two shafts were constructed using concrete composites having different amounts of pulverized coal combustion (PCC) fly ash and bottom ash. All the shafts had nominal diameter of 13 inches and were 25 feet deep. The shafts were installed and tested at a site located in the Carterville campus of Southern Illinois University Carbondale. The objective of the study was to demonstrate the suitability of concrete composites made with PCC fly ash and bottom ash for construction of drilled shaft foundations by conducting a set of lateral load-deflection tests on field-size drilled piers. Four drilled shafts were constructed using conventional concrete and PCC fly ash and bottom ash at a site in Carterville, Illinois and tested under lateral loads (The fourth shaft was used as a reaction shaft to apply the lateral loads). The two selected composites were: (1) 100 percent replacement of natural fine aggregate with PCC bottom ash and 10 percent replacement of portland cement with PCC fly ash (Specimen F10B100), and (2) 50 percent replacement of natural fine aggregate with PCC bottom ash and 20 percent replacement of portland cement with PCC fly ash (Specimen F10B50).

The site used for conducting the tests is located in the Carterville campus of Southern Illinois University Carbondale (SIUC). One of the borings was drilled to a maximum depth of 34 ft. The borings were drilled using a truck mounted CME 75 rotary drill. Standard Penetration Tests (SPT's) were performed using an

automatic hammer. The boring log and the associated standard penetration test results are shown in figure 1.21.

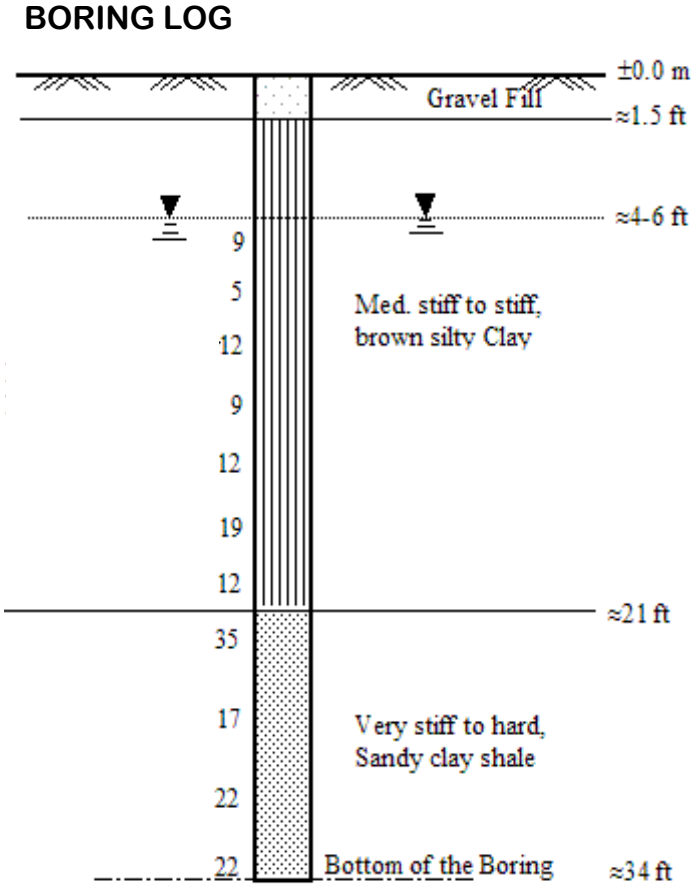

Figure 1.21 – Boring log at the test location. (Kumar, Kort, Hosin,Chong, 2004).

Based on the correlations presented in book titled "An Insight into the Theoretical Background of SSI" equation (40) for the SPT test results and the soil stiffness, the coefficient of subgrade reaction values are obtained for the soil layers which are tabulated in table 1.5.

Table 1.5 – Variation of coefficient of subgrade reaction with depth

Depth(ft)	N	k_n (kip/ft^3)	E (kip/ft^2)
0	0	0.0	0.0
2	9	63.1	126.3
4	9	63.1	252.5
7	5	35.1	239.5
10	12	84.2	813.1
12	9	63.1	788.5
15	12	84.2	1289.6
18	19	133.3	2419.0
21	12	84.2	1766.0
25	35	245.5	6206.5

The drilled shafts were tested 90 days after their construction to allow enough time for the piers to cure under field environmental conditions. The compressive strengths of the concrete mixes with curing age are tabulated in table 1.6.

Table 1.6 – Compressive Strengths (f'_c) of the Concrete Composites and Control Mix Used. (Kumar, Kort, Hosin,Chong, 2004).

Mixture Designation	Compressive Strength (psi) Curing Age (Days)				
	7	28	60	90	180
F10B100	2941	4647	5612	6069	7071
F20B50	3154	5113	7051	7174	7869
CM	4555	6342	7180	7222	7581

The elastic moduli for the mixes based on the 90day compressive strength are as follows:

Table 1.7 – Elastic modulus (90 days)

Mixture designation	E (ksf)
F10B100	639434
F20B50	695212
CM	700186

Figure 1.22 shows the elevation view of the 3-D FE soil model generated for the 13in diameter 25 ft deep shafts before and after the lateral loading is applied.

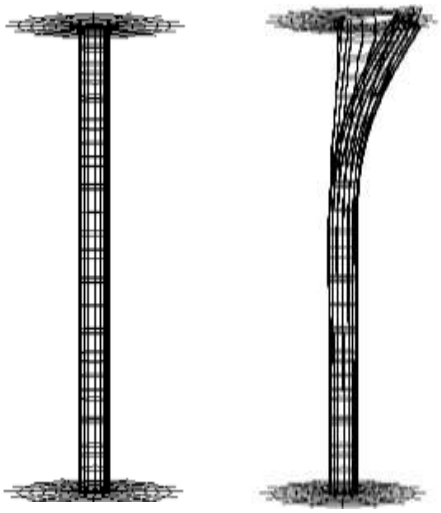

Figure 1.22 – 3-D FE model of the shafts tested by Kumar et.el (2004) before and after the lateral loading.

The finite element model was generated by the procedures developed in book titled "An Insight into the Theoretical Background of SSI". The model consists of a total of 2496 elements (480 C3D8R, 1520 C3D8, and 496 CIN3D8) with 9327 degrees of freedom.

The soil profile consists of cohesive material, thus the friction angle has been specified as zero and the elastic modulus has been taken as constant within these regions.

Figure 1.23 shows the experimental displacement values for the three test shafts under different lateral loadings. Figure 1.24 shows the displacement results from the 3D FE model.

Figure 1.25 are the comparison of the displacements from the experimental research by Kumar et.al (2004) and the results from the analytical results based on the finite element models developed in this thesis. The displacements from the FE analysis results are in good agreement with those from experimental results. The analytical model shows a lower stiffness and thus slightly higher displacement values than the experimental results since the soil selfweight deformation and the soil-structure interface friction have not been included in the model.

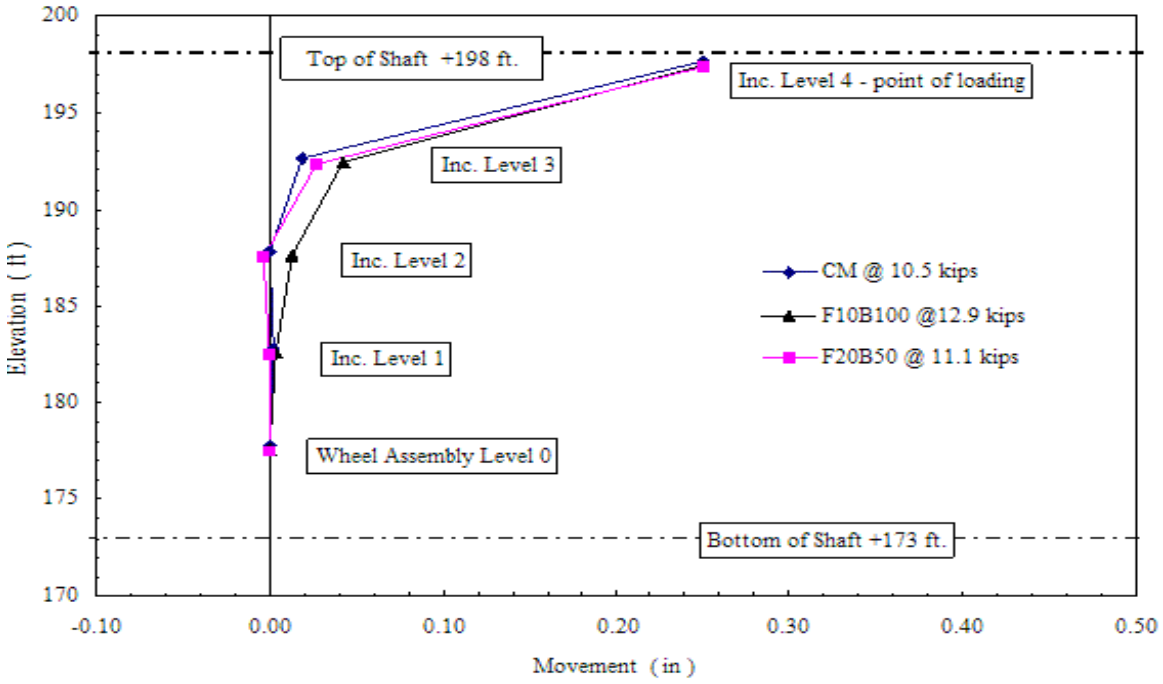

Figure 1.23 – Displacement values for the laterally loaded test shafts. (Kumar, Kort, Hosin,Chong, 2004).

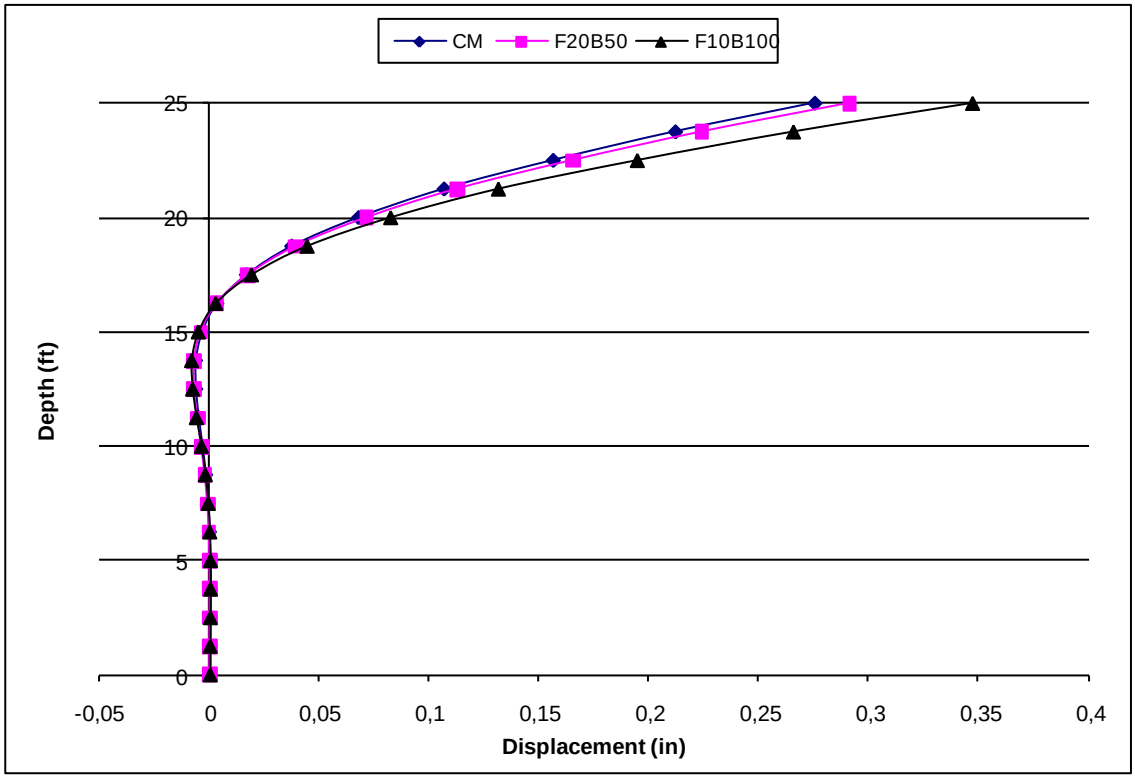

Figure 1.24 – Analytical (FEM) displacement values for the test shafts.

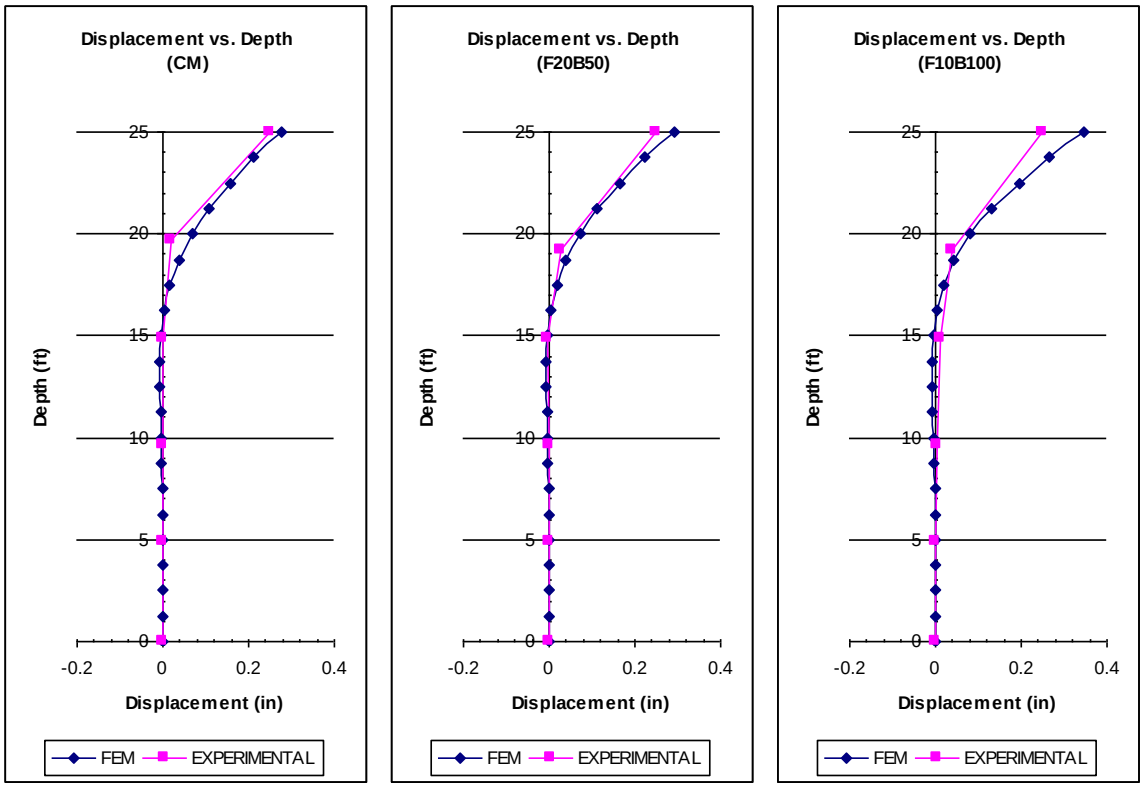

Figure 1.25 – Comparison of 3-D FEM results with existing the experimental data from Kumar et.al (2004).

The plots in figure 1.25 show a reasonable agreement between experimental and analytical results. The 3D FE model seems to predict reasonably the trend in shaft displacements near the top as well as the magnitude.

1.3.2 Doremus Avenue Bridge

The Doremus Avenue Bridse is located in Newark, NJ. The bridge foundations are concrete drilled shafts with steel casing with the following properties:

<u>concrete</u>
Class B
f_c' = 20 MPa
E_c = 21000 MPa
ρ = 2400 kg/m^3

<u>steel</u>
E_s = 200000 MPa
ρ = 7800 kg/m^3

The shafts are 25 meters in depth and extend 3 meters into the bedrock. The concrete diameter is 1.196 meters with a 0.012-meter thick steel casing (total shaft diameter is 1.22 meter). The center-to-center spacing of the shafts is 3.75 meters.
Balic M. and Gucunski N. (2002) conducted on-site lateral load tests on the drilled shafts during the construction stage of the deep foundations, which involved the use of a shaker that applied sinusoidal loads at specified frequencies. The load was applied to one of the shafts and the response of the loaded and adjacent shafts was measured using geophones, placed on the top of each shaft.
Soil-shaft interaction modifies shaft stiffness, which makes the shaft response dependent on the frequency of the loading. This has been investigated by many researchers such as Novak(1974) and Gazetas(1984). Novak et al. (1983) has shown that the shaft-soil system stiffness depends on the relative stiffness of the shaft and the soil, slenderness ratio of the shaft, shaft support condition and the variation of soil properties with the depth. The stiffness of the SSI system is also affected by the disturbance zone around the shaft, as well as the accumulated shaft-soil interface separations caused by repetitive loading in cohesive soils for soil depths 5-10 shaft diameters below the ground level (Novak, 1980).

Figure 1.26 shows the three dimensional solid and wireframe views of the group shaft. The model has been generated in a similar format to the shafts generated in chapter 5 of this dissertation. One major difference is the use of a steel shell around the concrete shafts. The use of steel shell around the concrete has the effect of increasing the bending stiffness of the shafts as well as modifying the interface friction with the soil.

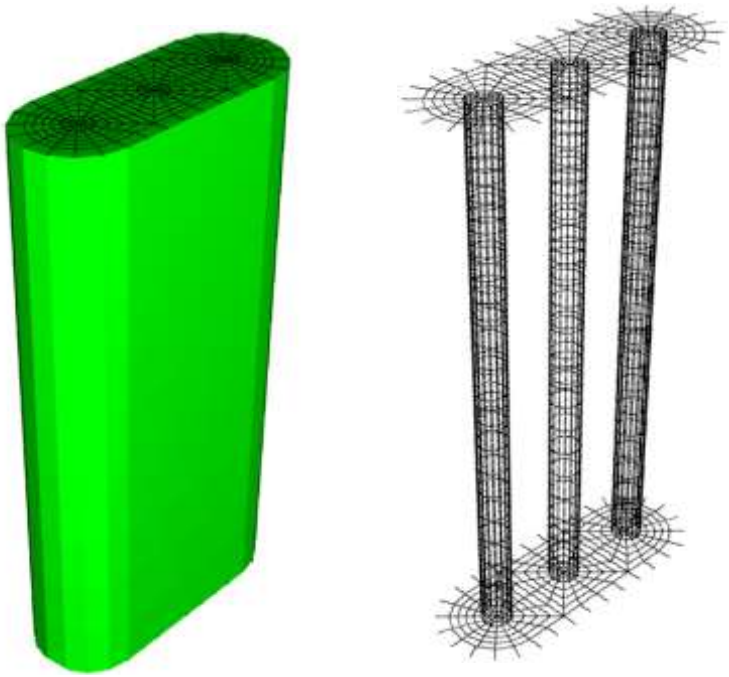

(a) Solid (b) Wireframe

Figure 1.26 – 3D solid and wireframe views of the Doremus group shaft.

S4R shell elements are used to model the steel shell. The shell and the concrete are rigidly connected to each other such that the shaft section responds as a composite structure. Figure 6.27 shows the plan view of the model showing the concrete core and the steel shells around the concrete cores. Figure 1.28 shows the soil profile and the stiffness parameters associated with the soil types along the profile. Table 1.8 is the soil stiffness parameters obtained by through shear wave testing.

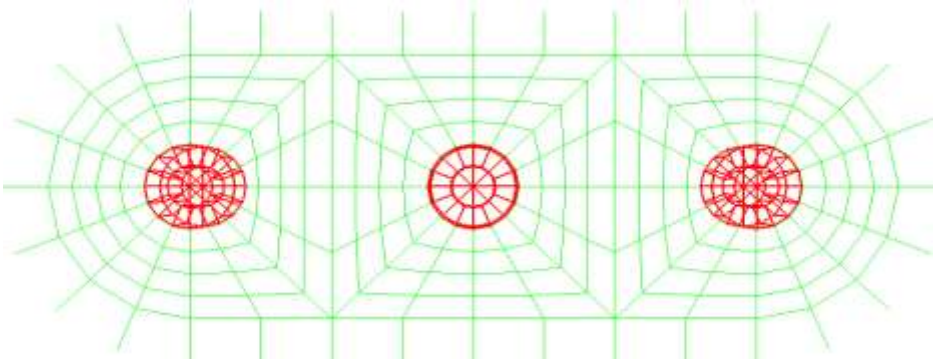

(a) Highlighted elements are the concrete cores of the shafts.

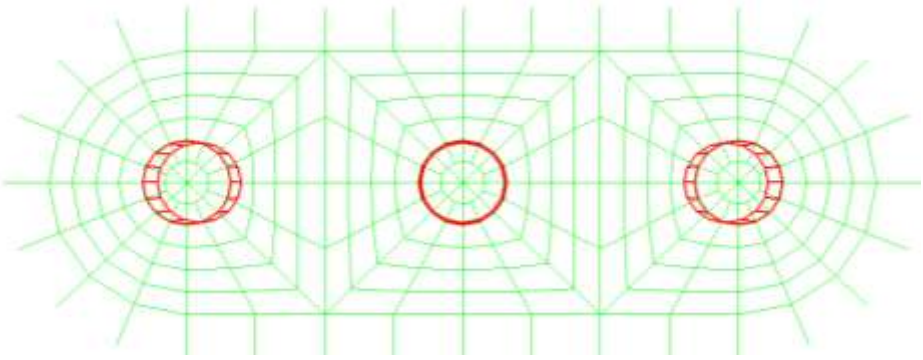

(b) Highlighted elements are the steel shells of the shafts.

Figure 1.27 – Plan view of the components of the shafts (a) Concrete cores, (b) Steel shells.

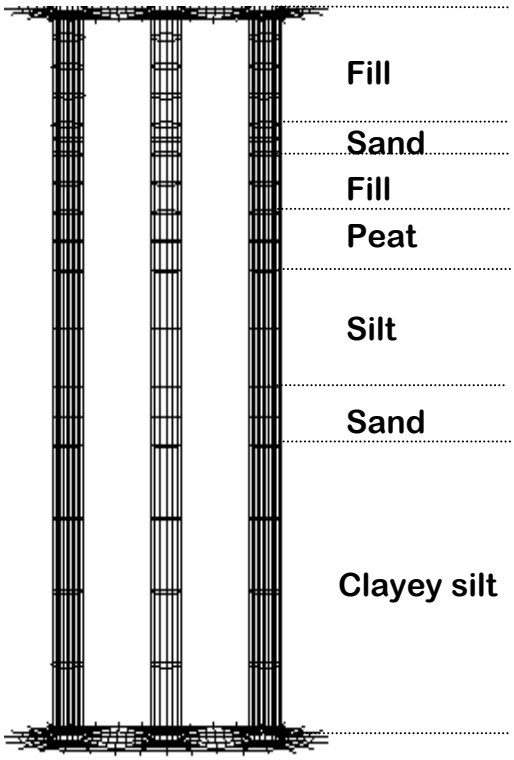

Figure 1.28 – Soil profile at Doremus group shaft location.

Table 1.8 – Soil profile at Doremus group shaft location (Balic, 2002)

depth (m)	soil type	unit weight (kN/m^3)	density (kg/m^3)	friction angle (°)	velocity (m/sec)	S. Modulus (N/m^2)	E. Modulus (N/m^2)
0	fill	19	1936.8	32.5	139	37420897.0	93552242.6
4	sand	19.6	1998.0	35	267	142432660.6	356081651.4
5	fill	9	917.4	32.5	170	26513761.5	66284403.7
7	peat	11.8	1202.9	0	183	40282385.3	100705963.3
9	silt	18.9	1926.6	0	256	126262018.3	315655045.9
13	sand	19.6	1998.0	35	360	258935779.8	647339449.5
15	clay/silt	18.9	1926.6	0	320	197284403.7	493211009.2
25	bedrock						

$$\text{shear wave velocity}: v_s = \sqrt{\frac{G}{\rho}} \qquad \text{shear modulus}: G = \frac{E}{2(1+\nu)} \qquad (1)$$

G=Shear modulus
E=Elastic modulus
υ=Poisson's ratio
ρ=density

The shafts were excited harmonically using an APS Model 400 electromagnetic shaker. The shaker was suspended on a frame and attached to the drilled shaft through a steel section anchored into the shaft. The force on the shaker was controlled by a signal generator and amplifier, and measured using a load cell placed between the arm of the shaker and the steel section. The response of the loaded and adjacent shafts was measured using triaxial Mark Products L-4C-3D geophones, placed on the top of the shaft. The test setup is shown in figure 1.29.

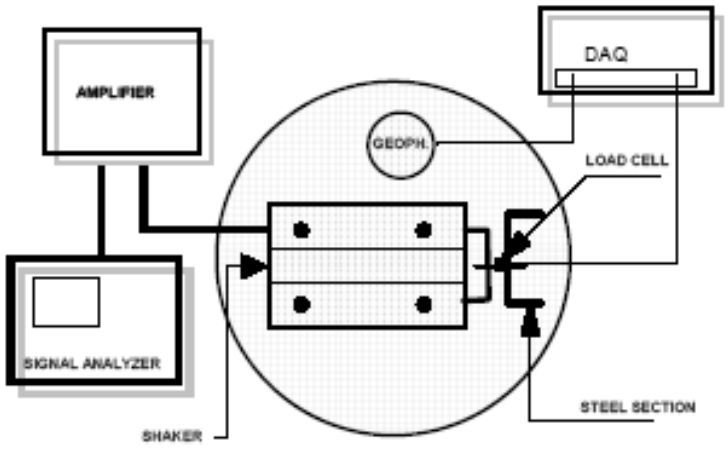

Figure 1.29 – Plan view of the experimental setup. (Balic, 2002)

Figure 1.30(a) shows the forcing function applied by the shaker. Figure 1.30(b) shows the sinusoidal approximation of the forces applied at various frequencies by the shaker in the analytical model. The sinusoidal approximation was necessary, since the forcing function shown in figure 1.30(a) could not be exactly defined. The displacements obtained through experimental testing and analytical modeling is shown in figure 1.31.

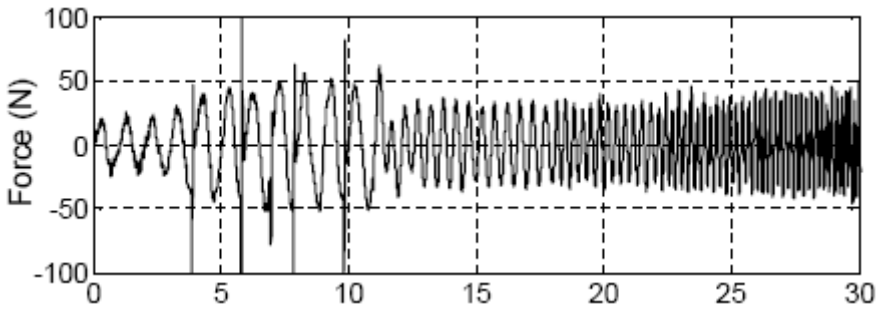

(a) – Loads applied by the electromagnetic shaker. (Balic, 2002)

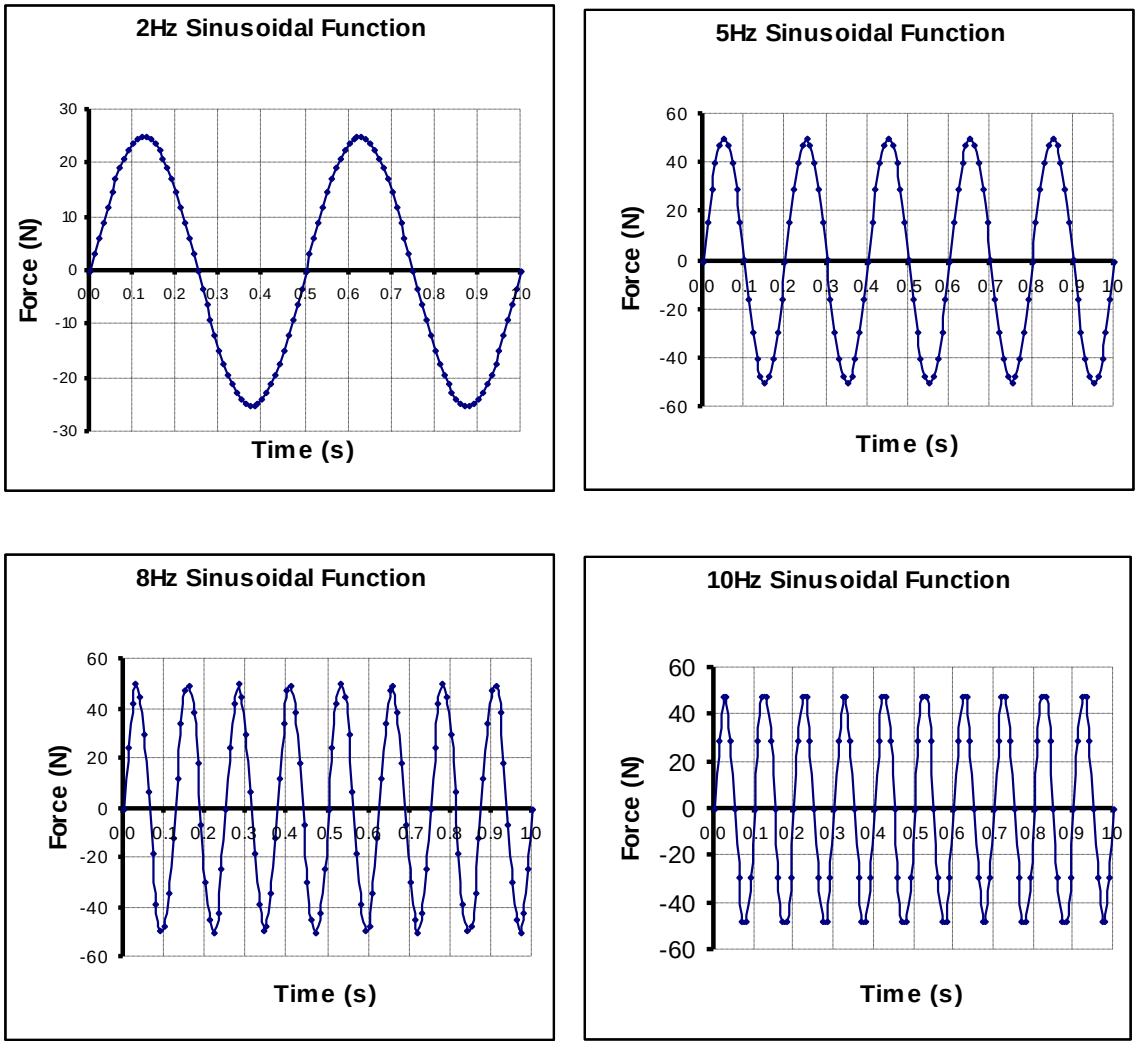

(b) –Sinusoidal forces applied by the FEM with varying frequencies.

Figure 1.30 – Dynamic loading applied by the shaker and the FE model.

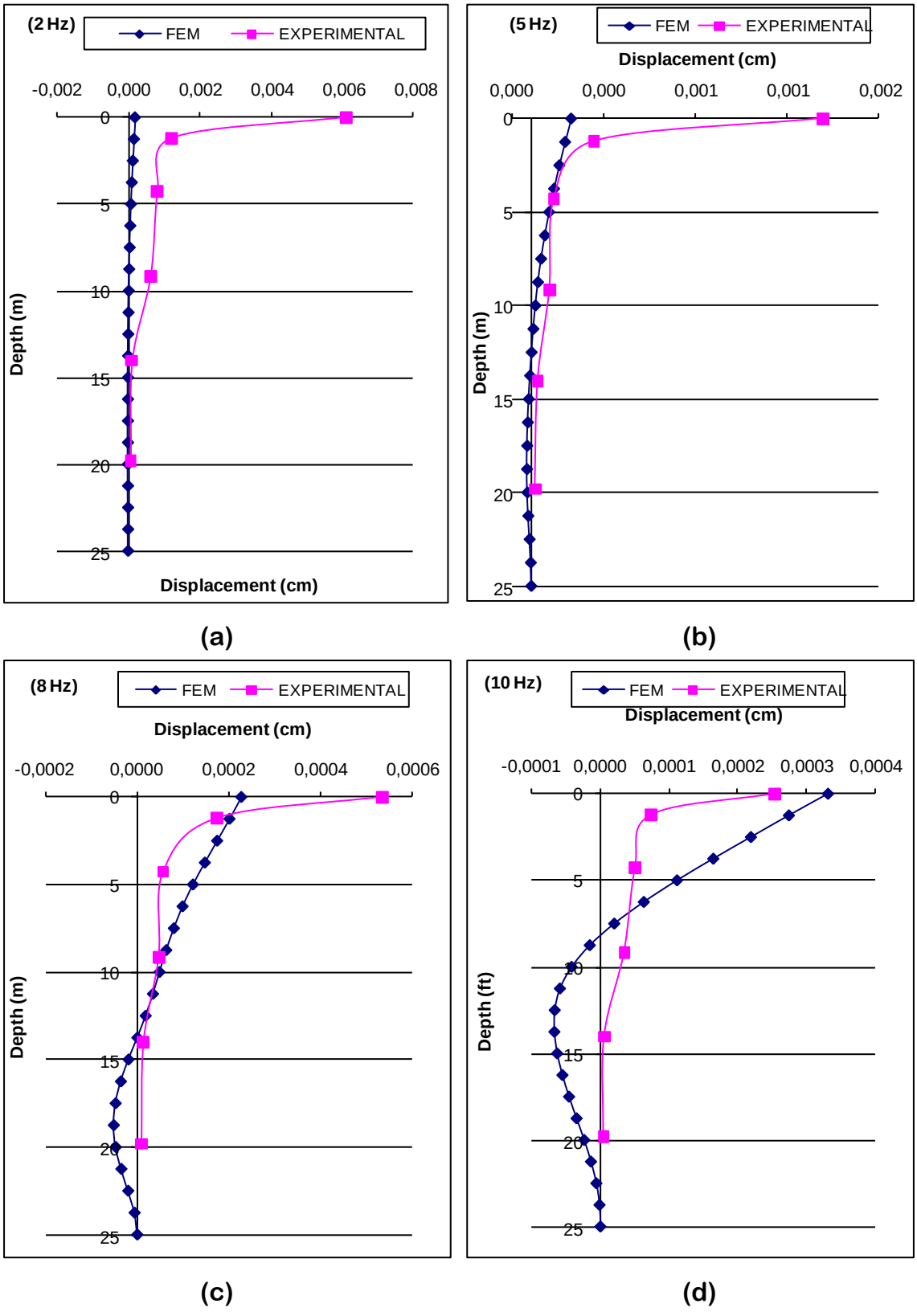

Figure 1.31 – Comparison of the experimental and the analytical results for various excitation frequencies.

From the experimental displacement profile, a large displacement is observed at the top of the shaft. The close proximity of the location where the displacement was measured to the shaker and the soil-structure interface separation is believed to be cause of this large displacement. The comparison of the experimental and the analytical results provide strong evidence that the shaft lacks the soil support due to shaft-soil surface separations. Further investigation into the site where the tests were conducted resulted in the findings and visual confirmation that there were significant shaft-soil surface separations as well as random fillings along a depth that extended a significant distance below the ground surface that couldn't be quantified at the time of testing (Balic, 2004). The drilling of the hole, and the placement of the steel casing that extends the full depth of the shaft, may have caused a significant reduction in the soil strength in close proximity to the shaft, as well as widening the hole beyond the design diameter. The impact of such a process would be to significantly reduce or completely diminish the soil support to the shaft under lateral loadings. On the other hand, the dynamic nature of the loading also modifies the response of the shaft based on the natural frequency of the soil-shaft system, which is dependent on the stiffness and the mass of the shaft and the soil.

The FE model was modified to incorporate such effects that were believed to be the cause of the differences between the experimental and the analytical results presented in figure 6.31. To this end, the soil interaction between the shaft and the soil was removed and the model was re-analyzed. The comparison of the experimental and the analytical results with the soil interaction removed is shown in figure 1.32.

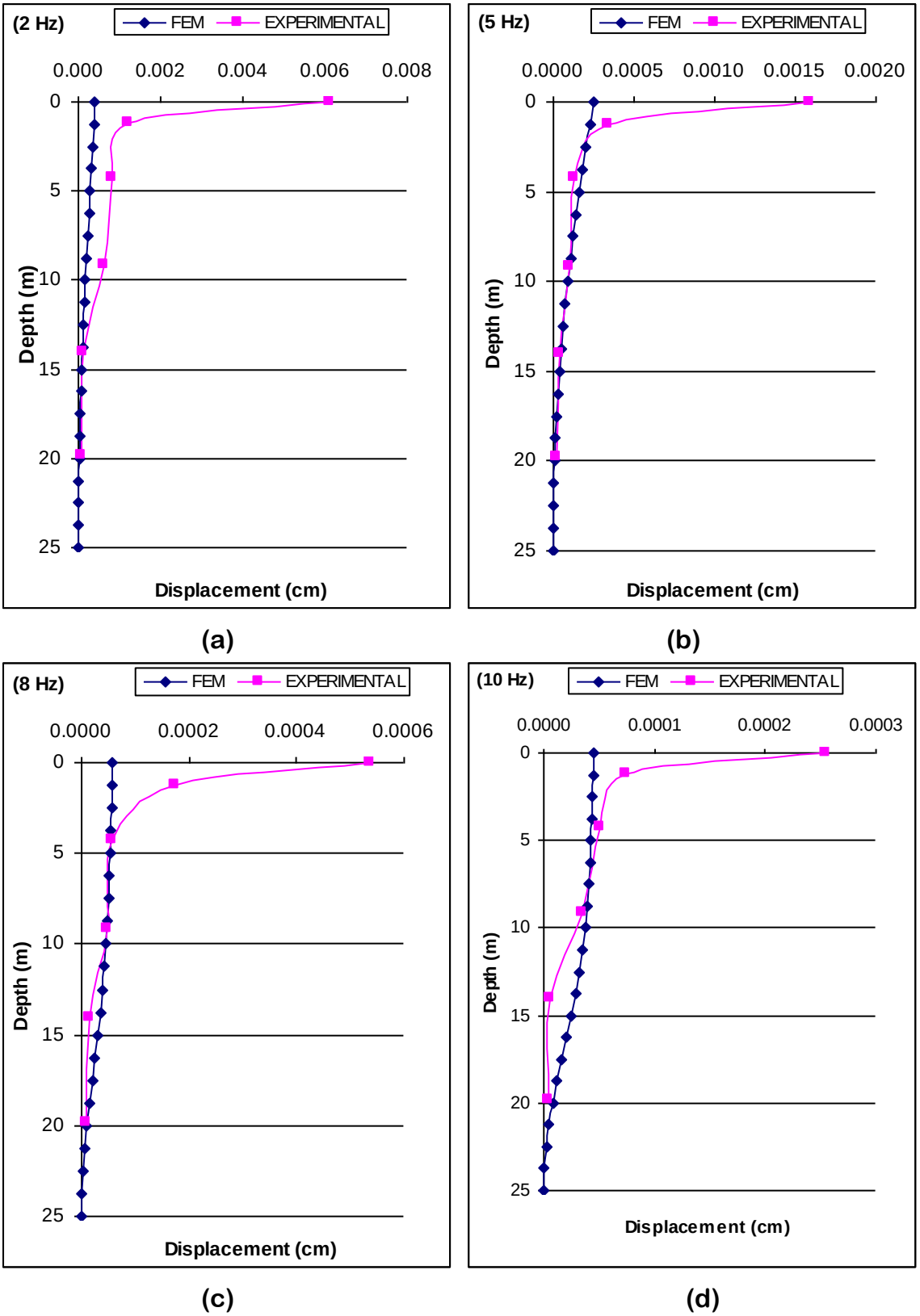

Figure 1.32 – Comparison of the experimental and the analytical results for various excitation frequencies with the soil interaction removed.

The removal of soil support resulted in analytical results in better correlation with experimental results. As the experimental evidence suggests, the analytical model showed that the stiff steel shell-concrete shaft resists the lateral load without the soil support.

Figure 6.33 shows the shaft displacements under dynamic loadings with different frequencies. Figure 6.34 shows the corresponding analytical displacement results. The displacement result at the ground level has been removed from figures 1.33 and 1.34.

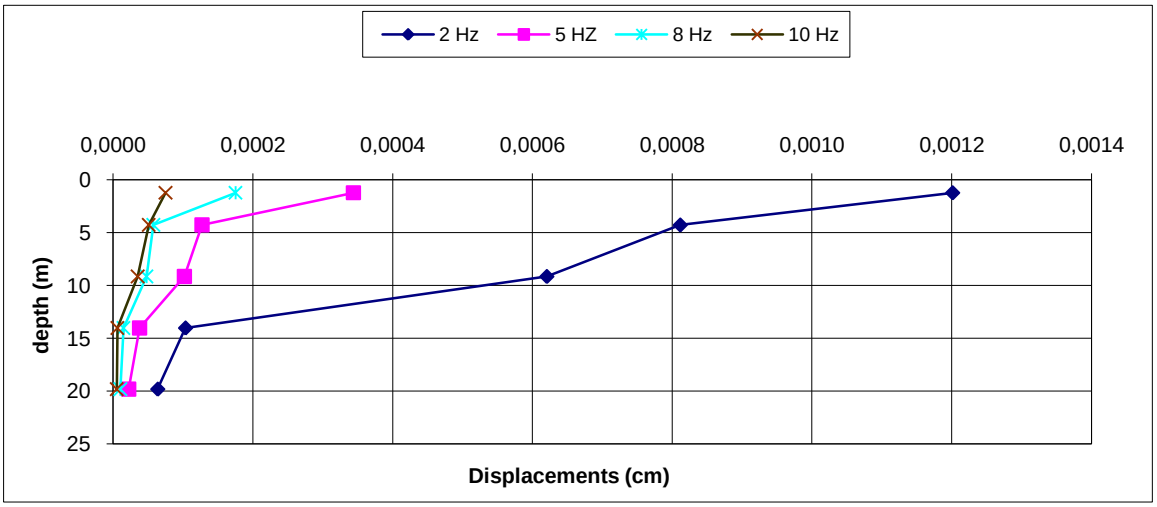

Figure 1.33 –Experimental displacement values along the shaft depth (Balic, 2004)

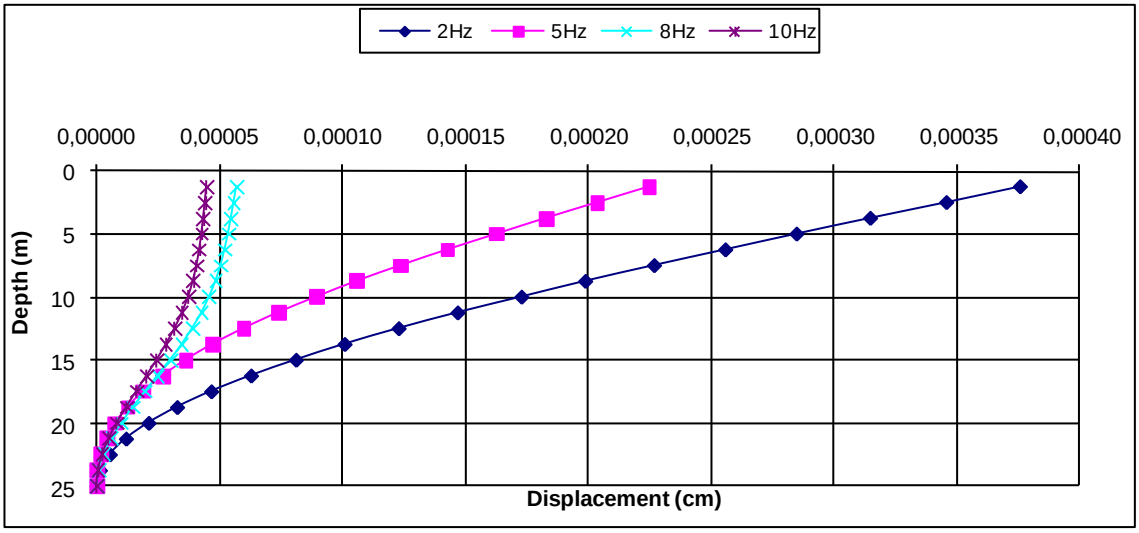

Figure 1.34 – Analytical displacement values along the shaft from FE modeling.

The analytical model has predicted the variation of the response of the shaft to cyclic loading similar to the experimental results. Due to the low natural frequency of the shaft, the lateral response for higher frequencies is lower.

REFERENCES

1. ABAQUS Standard/Explicit Manuals versions 6.3&6.4

2. Anderson, Townsend. (2002) “A Laterally Loaded Pile Database”. Deep Foundations 2002: An International Perspective on Theory, Design, Construction, and Performance pp. 262-273

3. Baker (1993). “Use of Pressuremeter in Mixed Highrise Foundation Design”. Design and Performance of Deep Foundations: Piles and Piers in Soil and Soft Rock pp. 1-13

4. Boulanger, Hutchinson, Chai, Idriss (2004). "Estimating Inelastic Displacements for Design: Extended Pile-Shaft-Supported Bridge Structures” Earthquake Spectra, Vol. 20, No. 4, pp. 1081-1094.

5. Bowles (1997). “Foundation Analysis and Design 5th Edition” MacGraw-Hill Companies

6. Briaud, Buchanan (2000) “Introduction to Soil Moduli”.

7. Briaud, L.L., Smith, T.D. Tucker, L. (1985). "Pressuremeter Design Method for Laterally Loaded Piles," Proceedings of the XI International Conference on Soil Mechanics and Foundation Engineering, San Francisco, CA, U.S.A.,

8. Briaud, Johnson, Stroman (1984). “Lateral Load Test of an Aged Drilled Shaft” Laterally loaded deep foundations: Analysis and performance, STP 835 pp. 172-181

9. Britto, Gunn, (1987) Critical State Soil Mechanics Via Finite Elements Ellis Horwood Limited

10. Chen, Liu (1990). “Development in Geotechnical Engineering 52 -Limit Analysis and soil plasticity” -Elsevier Publishing

11. Chen, Mizuno (1990) “Developments in geotechnical engineering53 -Nonlinear Analysis in Soil Mechanics Theory and Implementation”- Elsevier Publishing

12. Chen (1975) “Development in Geotechnical Engineering 7 -Limit Analysis and soil plasticity”- Elsevier Publishing

13. Choi, Oh, Kwon, Kim. (2002) “A Numerical Analysis for Axial and Lateral Behavior of Instrumented Steel Pipe Piles”. Deep Foundations 2002: An International Perspective on Theory, Design, Construction, and Performance pp. 289-304

14. Cook, Malkus, Plesha, Witt (2002). “Concepts and Applications of Finite Element Analysis 4th Edition” John Wiley and Sons Inc.

15. Dameron, Arzoumanidis, Bennett, Malik (1999). “Seismic Analysis and Displacement Based Evaluation of the Brooklyn-Queens Expressway”.

16. Das (1999) “Principles of Foundation Engineering 4th edition” PWS Publishing

17. Dessai, Abel (2002). “Introduction to Finite Element Modeling”. CBS Publishers & Distributers

18. Duggal, Bohinsky, Chu. (1989) “Comparative Performance of Two Pile Types” Foundation Engineering, pp. 943-956

19. Habigaghi, K. and Langer, J.A. (1984). “Horizontal Subgrade Modulus of Granular Soils”. Laterally loaded deep foundations: Analysis and performance, STP 835 pp. 21-34

20. Horvath, (1984). “Simplified Elastic Continuum Applied to the Laterally Loaded Pile Problem”. Laterally loaded deep foundations: Analysis and performance, Laterally loaded deep foundations: Analysis and performance, STP 835 pp. 229-238

21. Horvath J.S. (2002) “Soil-Structure Interaction Research Project:Basic SSI Concepts and Applications Overview” Report No. CGT-2002-2

22. Huang, Ye, Tang. (2002) “Dynamic Coupled Analysis for Earthquake Response of Pile Foundations”. Deep Foundations 2002: An International Perspective on Theory, Design, Construction, and Performance pp. 396-404

23. Kappos, Sextos (1999) “Effect of Foundation Type and Compliance on Seismic Response on RC Bridges”. Journal of bridge engineering, Vol.6, No.2, March 2001.

24. Kulhawy. (2002) “Observations on Some Shortcomings in Foundation Analysis and Design”. Deep Foundations 2002 (GSP 116), pp.1-5.

25. Kulhawy, Cushing.(2002) “Drained Elastic Behavior of Drilled Shafts in Cohesionless Soils”. Deep Foundations 2002: An International Perspective on Theory, Design, Construction pp. 22-36

26. Kulhawy, Agaiby, Trautmann (1996) "On large scale model testing of laterally loaded drilled shafts in sand " Geotechnical Testing Journal , vol.v19., no.n1., pp.pp32-40.

27. Kulhawy, F. H. (1991). “Drilled shaft foundations , Foundation engineering handbook”.

28. Kumar, Kort, Hosin, and Chong (2004) “Lateral Load Tests on Small Diameter Drilled Piers”

29. Kumar, Alizadeh (2002). “Lateral Load-Deflection Response of Single Piles in Sand”.

30. Kort, Kumar, Hosin, Ng (2002) "Lateral Load Tests on Small Diameter Drilled Piers".

31. Lin,Yang, Juang, Lee (2000). "Analysis of Laterally Loaded Piles in a Two-Layered Elastic Medium".

32. Lee, Kane, Bennett, Drumm (1989) "Investigation and Modeling of Soil-Structure Interface Properties"

33. Lee (1991) "Discrete Layer Analysis of Laterally Loaded Piles".

34. Long, Reese (1984). "Testing and Analysis of Two Offshore Drilled Shafts Subjected to Lateral Loads". Laterally loaded deep foundations: Analysis and performance, STP 835 pp. 215-228

35. Luna, Jadi (1998) "Determination of Dynamic Soil Properties Using Geophysical Methods".

36. Macklin, Nelson, Chou (1993) "A Lateral Load Test on Seven Foot Diameter Caissons".

37. Maharaj (1997)"Load-Deflection Response of Laterally LoadedSingle Pile by Nonlinear Finite Element Analysis".

38. Matlock, Reese, (1960). Generalized Solutions for laterally Loaded Piles, Journal of the Soil Mechanics and Foundations Division, ASCE, Vol.86, No SM5, Proc.Paper 2626, pp.63-91

39. Motan, Gabr. (1989) "A Flat-Dilatometer Study of Lateral Soil Response."

40. Neate (1983) "Augered Cast in Place Piles".

41. Neely (1979) "Bearing pressure-SPT Correlations for Expanded Base Piles in Sand".

42. Olson, Clifford, Wright (1983) "Nondestructive Testing of Deep Foundation with Sonic Methods".

43. Petek, Felice, Holtz. "Capacity Analysis of Drilled Shafts with Defects".

44. Pise, P. J. (1983), Lateral Response of Free-Head Pile, Journal of Geotechnical Engineering, ASCE, Vol. 109, No.8 pp. 1126-1131.

45. Popov (1998) "Engineering Mechanics of Solids 2nd Edition" Prentice Hall Publishing.

46. Prakash, Sharma (1990) "Pile Foundations in Engineering Practice". John Wiley and Sons Inc.

47. Puppala, Moalim (1986) "Evaluation of Driven Pile Load Capacity Using CPT Based LCPC and European Interpretation Methods".

48. Pyle, R. and Beikae, M. (1984). “A New Solution for the Resistance of Single Piles to Lateral Loading” Laterally Loaded Deep Foundations: Analysis and Performance, STP 835 835 pp. 3-20

49. Reese, Wright, Aurora (1984). “Analysis of a Pile Group Under Lateral Loading”. Laterally loaded deep foundations: Analysis and performance, STP 835 pp. 56-71

50. Reese, L.C., and Matlock, H., (1956). “Non-Dimensional Solutions for Laterally Loaded Piles with Soil Modulus Assumed Proportional to Depth”, Proceedings, Eighth Texas Conference on Soil Mechanics and Foundation Engineering,

51. Roberston, Hughes (1984). “Design of Laterally Loaded Displacement Piles Using a Driven Pressuremeter”. Laterally loaded deep foundations: Analysis and performance, STP 835 pp. 229-238

52. Sogge (1984). “Microcomputer Analysis of Laterally Loaded Piles”. Laterally Loaded Deep Foundations: Analysis and Performance, STP 835 pp. 35-48.

53. Smith, T.D., (1989) "Fact or Friction: A Review of Soil Response to a Laterally Moving Pile", Proceedings of the Foundation Engineering Congress, Northwestern University, Evanston, Illinois, pp. 588-598

54. Smith, T.D., Slyh, R. (1986) "Side Friction Mobilization Rates for Laterally Loaded Piles from the Pressuremeter, “ Proceedings of the Second International Symposium, The Pressuremeter and its Marine Application”, Texas A&M, May ASTM STP 950, pp. 478-491

55. Taciroglu, Rha, Stewart, Wallace, (1999). “Robust Numerical Models for Cyclic Response of Columns Embedded in Soil”.

56. Vennalaganti, Endley, Rao (1992) “Lateral Loads on Long piles and piers in granular soils”.

57. Wang, Rinne (1999) “Pile Foundation Construction Practice in Stiff Clays with Dense Granular Layers”.

58. Woodward, Gardner, Greer. (1972) “Drilled Pier Foundations” McGraw Hill Publishing

59. Zhang, Tulla, Grismala (1977) “Ultimate Resistance of Laterally Loaded Piles in Cohesionless Soils”.

60. Zafir (1986) “Seismic Foundation Stiffness for Bridges”.